

Aus der Klinik für Psychiatrie, Psychotherapie und Psychosomatik
Sektion Neuropsychologie
Lehr- und Forschungsgebiet Soziale und affektive Neurowissenschaften
(Leiter Juniorprofessor Dr. med. Dr. rer. nat. Danilo Bzdok)

Multivariate patterns of brain structure, brain function and symptoms in schizophrenia

Der Medizinischen Fakultät der Rheinisch-Westfälischen Technischen Hochschule Aachen vorgelegte Dissertation zur Erlangung des akademischen Grades eines Doktors der Theoretischen Medizin

von

Master sciences humaines et sociales

Jeremy Lefort-Besnard

aus Woippy (Frankreich).

Berichter: Juniorprofessor Dr. med. Dr. rer. nat. Danilo Bzdok
Universitätsprofessorin Dr. rer. nat. Kerstin Konrad

Tag der mündlichen Prüfung: 14. Februar 2019

List of publications

- Publications as a dissertation

1. Lefort-Besnard J., Bassett S.D., Smallwood J., Margulies S.D., Derntl B., Gruber, O., Aleman A., Jardri R., Varoquaux G., Thirion B., Eickhoff B.S., Bzdok D. Different shades of default mode disturbance in schizophrenia: Subnodal covariance estimation in structure and function; *Human Brain Mapping*; 2017, 39:644–661.
2. Lefort-Besnard J., Varoquaux G., Derntl B., Gruber O., Aleman A., Jardri R., Sommer I., Thirion B., Bzdok D. Patterns of Schizophrenia Symptoms: Hidden Structure in the PANSS Questionnaire; *Translational Psychiatry*; In press.

- Other publications

3. Fletcher-Watson S, Apicella F, Auyeung B, et al. Attitudes of the autism community to early autism research; *Autism*; 2017, 21(1): 61–74.
4. Fletcher-Watson S., Larsen K., Salomone E., and Members of the COST ESSEA Working Groups. What do parents of children with autism expect from participation in research? A community survey about early autism studies; *Autism*; 2017, DOI: 10.1177/1362361317728436.

Different shades of default mode disturbance in schizophrenia: Subnodal covariance estimation in structure and function

Jérémie Lefort-Besnard¹ | Danielle S. Bassett^{2,3} | Jonathan Smallwood⁴ |
Daniel S. Margulies⁵ | Birgit Derntl^{1,6,7} | Oliver Gruber⁸ | Andre Aleman⁹ |
Renaud Jardri¹⁰ | Gaël Varoquaux¹¹ | Bertrand Thirion¹¹ |
Simon B. Eickhoff^{12,13} | Danilo Bzdok^{1,6,11}

¹Department of Psychiatry, Psychotherapy, and Psychosomatics, RWTH Aachen University, Germany

²Department of Bioengineering, University of Pennsylvania, Philadelphia, Pennsylvania 19104, USA

³Department of Electrical and Systems Engineering, University of Pennsylvania, Philadelphia, Pennsylvania 19104, USA

⁴Department of Psychology, University of York, Heslington, United Kingdom

⁵Max Planck Research Group for Neuroanatomy and Connectivity, Max Planck Institute for Human Cognitive and Brain Sciences, Leipzig 04103, Germany

⁶Jülich Aachen Research Alliance (JARA) – Translational Brain Medicine, Aachen, Germany

⁷Department of Psychiatry and Psychotherapy, University of Tübingen, Germany

⁸Department of Psychiatry, University of Heidelberg, Germany

⁹BCN Neuroimaging Center, University Medical Center Groningen, University of Groningen, Groningen, The Netherlands

¹⁰Division of Psychiatry, University of Lille, CNRS UMR9193, SCALab & CHU Lille, Fontan Hospital, CURE platform, Lille 59000, France

¹¹Parietal Team, INRIA/Neurospin Saclay, France

¹²Institute of Systems Neuroscience, Heinrich-Heine University, Düsseldorf, Germany

¹³Institute of Neuroscience and Medicine (INM-7), Research Centre Jülich, 52425, Germany

Correspondence

Danilo Bzdok, Department of Psychiatry,
Psychotherapy, and Psychosomatics, RWTH
Aachen University, Germany. Email:danilo.
bzdok@rwth-aachen.de

Funding information

Deutsche Forschungsgemeinschaft (DFG),
Grant/Award Numbers: B22/2-1, B22/3-1,
and B22/4-1; International Research
Training Group, Grant/Award Number:
IRTG2150; Amazon AWS Research Grant
(2016 and 2017); The German National
Merit Foundation; START-Program of the
Faculty of Medicine, RWTH Aachen; John
D. and Catherine T. MacArthur Foundation;
The Alfred P. Sloan Foundation; The Army
Research Laboratory; The Army Research
Office, Grant/Award Numbers: W911NF-
10-2-0022 and W911NF-14-1-0679; The
National Institute of Mental Health, Grant/
Award Number: 2R01-DC-009209-11; The
National Institute of Child Health and
Human Development, Grant/Award Number:
1R01HD086888-01; The Office of
Naval Research; The National Science
Foundation, Grant/Award Numbers: BCS-

Abstract

Schizophrenia is a devastating mental disease with an apparent disruption in the highly associative default mode network (DMN). Interplay between this canonical network and others probably contributes to goal-directed behavior so its disturbance is a candidate neural fingerprint underlying schizophrenia psychopathology. Previous research has reported both hyperconnectivity and hypoconnectivity within the DMN, and both increased and decreased DMN coupling with the multimodal saliency network (SN) and dorsal attention network (DAN). This study systematically revisited network disruption in patients with schizophrenia using data-derived network atlases and multivariate pattern-learning algorithms in a multisite dataset ($n = 325$). Resting-state fluctuations in unconstrained brain states were used to estimate functional connectivity, and local volume differences between individuals were used to estimate structural co-occurrence within and between the DMN, SN, and DAN. In brain structure and function, sparse inverse covariance estimates of network coupling were used to characterize healthy participants and patients with schizophrenia, and to identify statistically significant group differences. Evidence did not confirm that the backbone of the DMN was the primary driver of brain dysfunction in schizophrenia. Instead, functional and structural aberrations were frequently located outside of the DMN core, such as in the anterior temporoparietal junction and precuneus. Additionally, functional covariation analyses highlighted dysfunctional DMN-DAN coupling, while structural covariation results highlighted aberrant DMN-SN coupling. Our findings reframe the role of the DMN core and its relation to

1441502, BCS-1430087, and NSF PHY-1554488; The Wellcome Trust, Grant/Award Number: 103817/Z/14/Z; The Volkswagen Foundation (Wandering Minds - 89440 and 89439); European Research Council (WANDERINGMINDS-646927)

canonical networks in schizophrenia. We thus underline the importance of large-scale neural interactions as effective biomarkers and indicators of how to tailor psychiatric care to single patients.

KEY WORDS

default mode network proper, functional connectivity, machine learning, neuroimaging, schizophrenia, sparse inverse covariance estimation, structural covariance, sparsity

1 | INTRODUCTION

Schizophrenia is one of the most devastating medical conditions, affecting ~1% of the general population across cultures (Salomon et al., 2013). The clinical manifestations of schizophrenia reflect the disruption of a variety of higher-order cognitive processes (D'Argembeau, Raffard, & Van der Linden, 2008; DeLisi, 2001; Frith & Corcoran, 1996; Haggard, Martin, Taylor-Clarke, Jeannerod, & Franck, 2003), which are likely to be subserved by the association cortex (Buckner & Krienen, 2013; Spreng, Mar, & Kim, 2009; Stephan et al., 2016). A collection of associative cortical areas commonly linked with higher-level cognitive processes in both health and schizophrenia is the default mode network (DMN).

Several investigators have shown that dysfunction of the DMN in schizophrenia is linked to many of the positive and negative symptoms, such as delusional experiences, hallucinations, and disorganization of thought and behavior (Bluhm et al., 2007; Camchong, Lim, Sponheim, & MacDonald, 2009; Garrity et al., 2007; Rotarska-Jagiela et al., 2010; Whitfield-Gabrieli et al., 2009). DMN dysregulation in schizophrenia has been associated with deficits in higher-order cognitive processes from different symptom clusters, ranging from attention to social cognition (Holt et al., 2011; Northoff & Qin, 2011; Whitfield-Gabrieli & Ford, 2012). While ~23% of variation in liability for schizophrenia can be explained by genetic risk variants (Lee et al., 2012; Ripke et al., 2014), evidence suggests that up to 40% of the interindividual variance in functional connectivity patterns of the DMN is under genetic control (Glahn et al., 2010), suggesting patterns of DMN organization to be a clinically useful biomarker of schizophrenia.

Evolutionarily, regions of the association cortex, including the DMN, have increased their spatial distance from sensory-motor areas, allowing cognition to become more decoupled from perception-action cycles, a view known as the "tethering hypothesis" (Buckner & Krienen, 2013). Indeed, the DMN was recently shown to be located at a maximum distance from sensori-motor regions in both functional and topographical space (Margulies et al., 2016). These findings help explain why the DMN is particularly important for maintaining and manipulating abstract representations from downstream multimodal brain systems (Andrews-Hanna, Smallwood, & Spreng, 2014; Buckner, Andrews-Hanna, & Schacter, 2008; Konishi, McLaren, Engen, & Smallwood, 2015; Raichle, 2015). Based on this integrative account of DMN function, its importance as a diagnostic measure for many of the features of schizophrenia may emerge through its abnormal interactions with other neural systems.

Understanding how large-scale networks subserve and control higher-order cognition is an emerging agenda in psychiatric research (Jang et al., 2017; Medaglia, Lynall, & Bassett, 2015). In particular, reorganization of the coupling modes between the DMN, saliency network (SN), and dorsal attention network (DAN) has been repeatedly proposed to carry information about the cognitive states that is complementary to task-related neural activity increases and decreases in the same network (Bzdok et al., 2016b; Margulies et al., 2016). Therefore, this study systematically explored the dysfunctional couplings between the DMN, SN, and DAN in schizophrenia (White, Joseph, Francis, & Liddle, 2010; Woodward, Rogers, & Heckers, 2011).

Abnormal connectivity between large-scale networks and the DMN can provide insight into the longstanding "disconnection hypothesis" that explains schizophrenia pathophysiology as coupling impairments due to context-dependent synaptic modulation (Friston, Brown, Siemerlus, & Stephan, 2016; Friston & Frith, 1995; Stephan et al., 2009a; Weinberger, Berman, Suddath, & Torrey, 1992). According to this pathophysiological concept, interregional coupling might be aberrant in schizophrenia because of impaired connectional pathways. For instance, it has been proposed that the strength of dopaminergic projections to canonical brain networks is altered in schizophrenia (Lewis & Gonzalez-Burgos, 2006; Stephan et al., 2009). Such disconnection of large-scale networks may contribute to positive symptoms through the failure of attentional reallocation and monitoring processes, but also to cognitive symptoms through impaired perceptual inference and disturbance of associative learning, as well as to negative symptoms due to inability of learning from and adapting to social environments. Together, these converging lines of evidence highlight that coupling patterns of canonical networks and the DMN may serve as an important biomarker for many aspects of the psychopathology of schizophrenia.

Although prior studies have highlighted the DMN as important in schizophrenia, the results have revealed a multifaceted and often inconsistent picture of how this large-scale network links to the major psychiatric disorder. Several studies have reported hypoconnectivity between regions of the DMN, such as between the posteromedial cortex (PMC) and the temporoparietal junctions (TPJ; Bluhm et al., 2007; Camchong, Lim, Sponheim, & MacDonald, 2011; Pankow et al., 2015). Other investigators instead reported hyperconnectivity within the DMN, such as between the medial prefrontal cortex and the PMC (Whitfield-Gabrieli et al., 2009; Zhou et al., 2007). Frequently inconsistent findings have also been published on pathological connectivity between the DMN and other commonly observed multimodal networks. For example, coupling of the DMN with the DAN as well as coupling between the DMN and the SN were reported as

pathologically decreased by some (White et al., 2010; Woodward et al., 2011) and as pathologically increased by others (Manoliu et al., 2013). Contradictory neural coupling findings have therefore been reported within the DMN of schizophrenia patients, as well as between the DMN and the other major brain networks including SN and DAN.

Given their intimate neurophysiological relationships and importance for disease, we studied the DMN and its pattern of coupling with the multimodal DAN and SN in schizophrenia adopting a comprehensive analysis strategy. First, because richer brain signals will be measured by taking into account the functional heterogeneity within the DMN at the subregional level, we deployed fine-grained topographical definitions from a recently completed DMN atlas as the (regions of interest (ROIs); Bzdok et al., 2013, 2015, 2016a; Eickhoff, Laird, Fox, Bzdok, & Hensel, 2016). Second, we extended the previous functional connectivity analyses between network parts to sparse inverse covariance estimation (Friedman, Hastie, & Tibshirani, 2008), which has recently been adapted for use in neuroimaging (Varoquaux, Gramfort, Poline, & Thirion, 2010). This under-exploited statistical framework, combined with benefits of using a large data-set, (i) offered increased interpretability by removing unimportant coupling relations, (ii) acknowledged the entire set of coupling relations instead of considering only pairs in isolation, and (iii) could account for the impact of third-party influences on each coupling relation. Third, the modeling approach is sufficiently abstract to allow for analogous analyses of the relationship between networks in both the functional (resting-state connectivity) and the structural (interindividual differences in brain volume) domain. Quantifying these aspects of structure-function correspondence underlying DMN aberration in schizophrenia aimed to complement previous connectivity investigations. We hypothesized that structural and functional interactions of DMN subnodes with two major brain networks provide insights into the mechanisms underlying schizophrenia psychopathology. That is, we expected the comparable quantification of neural network coupling in brain volume and function to allow zooming in on the multi-level disturbances underlying schizophrenia. This comprehensive analysis agenda allowed the formalization of complex correspondence between the neurobiological endophenotype and the clinical exophenotype in schizophrenia spectrum disorders.

2 | MATERIALS AND METHODS

2.1 | Data resources

This study considered magnetic resonance imaging (MRI) data from five different population samples acquired in Europe and USA: Aachen, Goettingen, Groningen, Lille, and COBRE. Resting-state functional connectivity (RSFC) and voxel-based morphometric (VBM) data were collected from a total of 482 participants, 241 patients with schizophrenia and 241 healthy controls. Given the present goal to directly compare functional brain recordings and structural brain scans, we further considered only those participants who provided both RSFC and VBM in the database. These control and disease groups ($n = 325$) were matched for age within and across sites (see Supporting Information

Table S1 for details). No participant in the healthy group had a record of neurological or psychiatric disorders. Each participant in the schizophrenia group had been diagnosed by a board-certified psychiatrist in accordance with the clinical criteria of the International Classification of Diseases (ICD-10) or the Diagnostic and Statistical Manual of Mental Disorders (DSM-IV-TR). All acquisition sites used 3T MRI scanners (see Supporting Information Table S2 for details). For the acquisition of functional brain maps (i.e., RSFC), fMRI scans of blood-oxygen-level-dependent (BOLD) signal were recorded from the participants who were instructed to lie still during the scanning session and to let the mind wander. A post-scan interview confirmed that participants adhered to these instructions and did not fall asleep. For the acquisition of structural brain maps (i.e., VBM), 3D T1 MRI scans were recorded from each participant. All participants gave written informed consent to participate in the study, which was approved by the ethics committee of the RWTH Aachen University, Germany. Note that all phenotypic information has been anonymized for tabulation.

2.2 | Brain function: Resting-state fMRI

To measure functional activity of brain regions, we analyzed resting-state EPI (echo-planar imaging) scans from standard BOLD acquisitions (see Supporting Information Table S2 for details). The preprocessing was performed in SPM8 (Statistical Parametric Mapping, Wellcome Department of Imaging Neuroscience, London, UK, <http://www.fil.ion.ucl.ac.uk/spm/>) run under MATLAB R2014a (Mathworks, Natick, MA). The first four brain scans were discarded to allow for magnetic field saturation. The EPI images were corrected for head movement by affine registration using a 2-pass procedure. To further reduce spurious correlations induced by motion, variance that could be explained by the head motion was removed from each voxel's time series. In particular, in adherence to previously published evaluations (Chai, Castanon, Ongur, & Whitfield-Gabrieli, 2012; Satterthwaite et al., 2013), we removed nuisance signals according to: (a) the 6 motion parameters derived from the image realignment, (b) their first derivatives, and (c) the respective squared terms (i.e., 24 parameter regression). These corrections have been shown to increase specificity and sensitivity of functional connectivity analyses and to detect valid signal correlation at rest. Motion correction was applied in all analyses. We did not perform global signal regression. Finally, the signal time series were band-pass filtered to preserve frequencies between 0.01 and 0.08 Hz, which have previously been associated with fluctuations of neuronal activity (Fox & Raichle, 2007; Lu et al., 2007), and are least impacted by physiological artifacts such as heart rate and respirations.

2.3 | Brain structure: Voxel-based morphometry (VBM) MRI

To measure the local brain volume across individuals, a high-resolution anatomical image was acquired from each participant using conventional scanning sequences. Anatomical scans were preprocessed with the VBM8 toolbox (<https://dbm.neuro.uni-jena.de/vbm>) in SPM8 using standard settings (DARTEL normalization to the ICBM-152 template,

affine and non-linear spatial normalization). Within a unified segmentation model (Ashburner & Friston, 2005), the brain scans were corrected for bias-field inhomogeneities. The brain tissue was segmented into gray matter, white matter, and cerebrospinal fluid, while adjusting for partial volume effects. We performed nonlinear modulation of segmented images to account for the amount of expansion and contraction applied during normalization using the nonlinear only modulation function within the VBM8 toolbox. The ensuing adjusted volume measurements represented the amount of gray matter corrected for individual brain sizes.

2.4 | Regions of interest

The DMN is essentially composed of four areas (which we henceforth refer to as network nodes), including the dorsomedial prefrontal cortex (DMPFC), the PMC, as well as the left and right TPJs (Buckner et al., 2008; Raichle et al., 2001). We note that the common approach is to examine the DMN with these nodes as targets of investigation (Du et al., 2016; Greicius, Krasnow, Reiss, & Menon, 2003; Whitfield-Gabrieli & Ford, 2012), assuming that the nodes of the DMN are functionally homogeneous. Nevertheless, the functional contribution of each individual node to the various abstract cognitive processes maintained by the overall network remains inconclusive (cf. Andrews-Hanna, Reidler, Sepulcre, Poulin, & Buckner, 2010; Bado et al., 2014; Braga & Buckner, 2017). Indeed, there is recent empirical evidence that the individual nodes of the DMN segregate into distinct subnodes (Schurz, Radua, Aichhorn, Richlan, & Perner, 2014). There is now accumulating support that neurobiologically meaningful subdivisions within each node of the DMN exist and could be profitably studied in the context of both healthy and abnormal human brain physiology.

Indeed, in a series of recent data-driven studies, the individual nodes of the DMN have been segregated into distinct subnodes based on local differences in functional interaction patterns with the rest of the brain, an established analysis technique called connectivity-based parcellation (Behrens et al., 2003; Eickhoff, Thirion, Varoquaux, & Bzdok, 2015). This technique assumes that a ROI may be divided into distinct subregions based on its whole-brain connectivity profiles. For each considered DMN node, connectivity-based parcellation has previously demonstrated a subdivision of the ROI into clusters with topographical boundary definitions, which can be reused in other studies.

Based on coherent whole-brain coupling profiles, the DMPFC was decomposed into two caudal and two rostral subnodes (Eickhoff et al., 2016). The PMC was partitioned into a ventral and dorsal subnode in the posterior cingulate cortex, one in the retrosplenial cortex (RSC) and one in the precuneus (Bzdok et al., 2015). Finally, the left and right TPJs of the DMN were decomposed into an anterior and a posterior subnode (Bzdok et al., 2013, 2016a). Adopting such a fine-grained perspective on DMN organization may provide new insights into the pathophysiology of schizophrenia. These node and subnode definitions of the DMN were used as three different ROI sets (cf. Supporting Information Table S3):

- First, we used the DMN atlas with the DMPFC, PMC, and both TPJs as composite nodes (4 ROIs), each collapsing its constituent subnodes (Figure 1a). The covariation analyses based on this ROI set examined the DMN at the conventional level of granularity: that is of network nodes. This served as a point of comparison for how this major brain network has most frequently been studied in previous brain-imaging research.
- Second, we used the full DMN atlas (12 ROIs) where the DMPFC, PMC, and the TPJs are represented as more fine-grained subnodes (Figure 1b). The DMPFC was segregated into a left and right caudal subnode and a rostro-ventral and rostro-dorsal part (left and right cDMPFC, rvDMPFC, and rdDMPFC). Note that among the midline structures of the DMN, only the DMPFC yielded a division along the right versus left hemisphere in our DMN subnode atlas. The left and right TPJs were partitioned into an anterior and posterior subnode (left and right aTPJ and pTPJ). The PMC was parcellated into four subnodes, including the precuneus (PREC), the ventral and dorsal posterior cingulate cortex (vPCC and dPCC), and the RSC. The corresponding covariation analyses tested the hypothesis that the DMN can be shown to reveal richer structure in brain signals when measured by conventional MRI scanners at the level of network subnodes.
- Third, the DMN subnode atlas (12 ROIs) was supplemented by nodes from two multi-modal networks (Figure 1c): (i) the SN (Bzdok et al., 2012), including the midcingulate cortex (MCC), the bilateral anterior insula (AI) and the amygdala (AM), and (ii) the DAN (Rottschy et al., 2012), including the dorsolateral prefrontal cortex (DLPFC) and the intraparietal sulcus (IPS) bilaterally (9 additional ROIs outside of the DMN). Covariation analyses here examined the hypothesis that the DMN subnodes also display characteristic interactions with the nodes of other canonical brain networks. Indeed, the DAN and the SN have been implicated in attentional switching and reallocation of focus, processes that are markedly disrupted in schizophrenia (Luck & Gold, 2008; Maruff, Pantelis, Danckert, Smith, & Currie, 1996; Menon & Uddin, 2010; Potkin et al., 2009; Sato et al., 2003).

In sum, the covariation analyses of functional coupling (RSFC) and volumetric coupling (VBM) performed in this study were based on three different sets of previously established ROI. Collectively, the analyses are used to probe the DMN at different neuroanatomical resolutions and to systematically evaluate their relations to other major brain networks. All of the ROIs used in this study are available online for transparency and reuse via a NeuroVault permanent link (<http://neurovault.org/collections/2216/>).

2.5 | Signal extraction

Using the three sets of ROIs described above, quantitative measures of functional activity and gray-matter volume differences were extracted within the DMN, DAN, and SN ROIs in every participant. Note that all analyses were constrained to these ROIs. For extracting relevant signal from a functional or structural brain scan, the ROIs served as

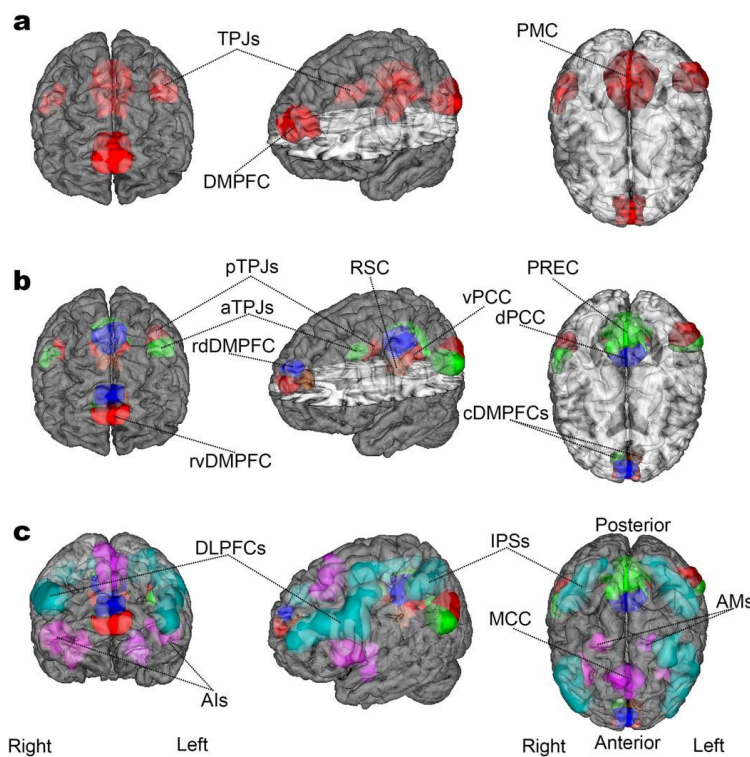


FIGURE 1 Target network definitions. The ROIs are rendered on the MNI standard brain with frontal, diagonal, and top views. (a) The DMN is represented by 4 ROIs, according to how the main network nodes are frequently studied in neuroimaging research. These comprise the DMPFC, PMC, and right/left TPJ. (b) The DMN nodes are subdivided into 12 ROIs accounting for the distinct subnodes in the DMN that were recently established (Bzdok et al., 2013, 2015, 2016a; Eickhoff et al., 2016). According to this prior work, the organizational core of the DMN ("DMN proper") likely corresponds especially to its blue and red subnodes (the ventral and the dorsal PCCs, the left and right posterior TPJs, and the rostralventral and rostrodorsal DMPFC). (c) The DMN subnodes are supplemented by 9 ROIs for the DAN (light green) and SN (purple), drawn from published quantitative meta-analyses (Bzdok et al., 2012; Rottschy et al., 2012). The DAN was composed of the DLPFC and IPS bilaterally. The SN included the MCC and the bilateral AI as well as AM. NeuroVault permanent link to all ROIs (21 in total) used in this study: <http://neurovault.org/collections/2216/>

topographic masks used to average the MRI signal across the voxels belonging to a given ROI. In RSFC, each target region was represented by the average BOLD signal across all voxels of that ROI. This feature-engineering strategy yielded as many functional brain variables as target regions in the ROI set for the participants. In VBM, each target region in the respective set of ROIs was represented by the average gray matter volume across all ROI voxels. Analogously, this way of engineering morphological brain features yielded as many volumetric brain variables per participant as the total number of ROIs in the current set. All ROI-wise functional or structural time series were transformed into z-scores by mean centering and unit-variance scaling. As part of the confound-removal procedure, variance that could be explained by the factors "site," "age," and "gender" as well as their two-way interactions was regressed out from the corresponding features.

2.5.1 | Measuring network covariation: Sparse inverse covariance estimation

Covariance has been argued to be a key notion when estimating the statistical dependencies characteristic of small-scale neural circuits and large-scale brain networks (Horwitz, McIntosh, Haxby, & Grady, 1995). In this study, we have performed formal inference of salient covariance relations in functional (i.e., RSFC) and volumetric (i.e., VBM) networks (or graphs, mathematically speaking) using sparse inverse covariance estimation. The automatic identification of networked organization in graphical models is an important step supporting the transition from descriptive statistics such as Pearson's correlation coefficient to generative models that capture higher-order interactions. Here, the employed statistical estimator represents an adaptation of Lasso-like regression models (Tibshirani, 1996) to Gaussian graphical models

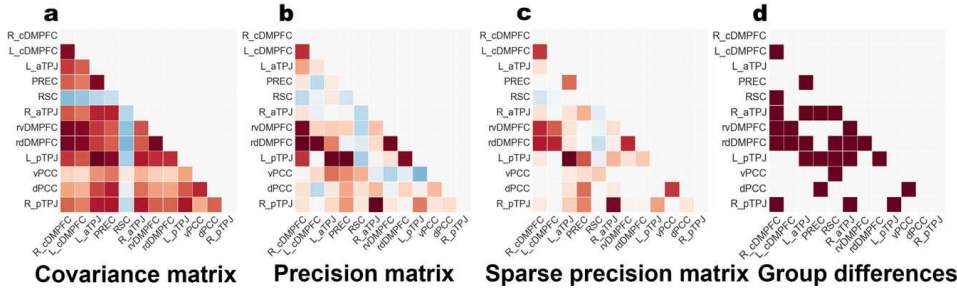


FIGURE 2 Network analysis workflow. Exemplary results illustrate the rationale of the statistical modeling framework. (a) The covariance matrix was computed with brain signals extracted from the DMN atlas. Each entry in this matrix indicates the linear relationship of each specific pair of target DMN nodes. (b) The precision matrix was computed by inverse covariance estimation (in this case without sparsity constraint). In contrast to the covariance matrix, the precision matrix captures the multiple relations between each of the pairs of target nodes while conditioning on the potential influence from the respective other nodes. (c) The parsimonious variant of the precision matrix was computed by sparse inverse covariance estimation with sparsity constraint. The additional modeling constraint improves interpretability by automatically reducing the network graph to the important network edges (non-zero strength, red or blue) and ignoring the irrelevant ones (zero strength, white). (d) The sparse precision matrices were computed separately in healthy controls and schizophrenic patients. Statistically significant group differences in coupling strengths (brown squares) were determined by nonparametric hypothesis testing. A significance test assessed group differences between all network relations at once. The entire analysis process was repeated for different network graph definitions (4 vs. 12 vs. 21 target nodes) and different imaging modalities (resting-state connectivity versus structural morphology).

(Friedman et al., 2008), an approach that has recently been adapted for application to neuroimaging data (Varoquaux et al., 2010). The validity of the derived probabilistic descriptions of the coupling properties in DMN function and volume was ascertained by cross-validation (three folds). These schemes ensured pattern generalization by measuring the goodness of fit in unseen data as a proxy for extrapolation to the general population (Shalev-Shwartz & Ben-David, 2014). This approach facilitated model selection for hyperparameter choice with an iteratively refined grid based on the log-likelihood score on left-out brain data (default parameters were chosen according to Varoquaux et al., 2010).

In a first step, we have computed the empirical covariance matrix (Figure 2a). This simple second-order statistic reflects how strongly the times series of ROI pairs covary (in terms of functional coupling in the RSFC analysis or volumetric coupling in the VBM analysis). The empirical covariance matrix is given by

$$\hat{\Sigma}_{\text{sample}} = \frac{1}{n} \chi^T \chi,$$

where $\chi \in \mathbb{R}^{n \times p}$ denotes the input dataset with p variables (i.e., functional brain signals averaged per ROI for the RSFC analysis and structural brain signals averaged per ROI for the VBM analysis) and n samples (i.e., brain scans). $\chi^T \chi$ denotes the inner product, the multiplication of the matrix χ with its transpose χ^T . The signed values in the covariance matrix indicate the direction of the linear relationship between two variables. This way of capturing the covariation in signal amplitude between any two ROIs was computed without statistically acknowledging the possible influence from the other ROIs. Every individual value in the covariance matrix can be viewed as a Pearson's linear correlation between each pair of ROIs, provided that the time series X were mean-centered and unit-variance scaled. Although the

strengths of correlation between time series of ROI pairs were considered in isolation, these covariation strength estimates were likely to be confounded with each other. For instance, a strong influence of ROI 1 on both ROI 2 and ROI 3 would entail high estimates of covariation between ROI 2 and ROI 3. This confound in the correlation structure between any two given target regions may therefore not accurately recover the underlying population-level coupling strength.

In a second step addressing this confound and enhancing neurobiological interpretability, we computed the partial correlations via the mathematical inverse of the covariance matrix, the so-called precision matrix (Figure 2b). The optimization objective is expressed by

$$\hat{K}_{\ell_1} = \operatorname{argmin}_{K > 0} \operatorname{tr}\left(K \hat{\Sigma}_{\text{sample}}\right) - \log \det K + \lambda \|K\|_1,$$

where $\hat{\Sigma}_{\text{sample}}$ is the empirical covariance matrix, $\|\cdot\|_1$ denotes the regularization constraint of putting an ℓ_1 norm on the matrix elements lying off the diagonal of the precision matrix K , and λ controls the amount of this sparsity constraint. In contrast to ordinary linear correlation or to the empirical covariance matrix described above, this matrix estimates the covariation between every two ROIs while conditioning on the potential influence of the remaining regions. In other words, the precision matrix obtains the direct covariation between two nodes within and between the DMN, SN, and DAN by accounting for partial correlations (Marrelec et al., 2006); unlike common linear correlation approaches, it does not privilege polysynaptic coupling patterns. Coming back to our toy example, we would thus obtain the conditionally independent proportion of covariation strength between ROI 2 and ROI 3 that is not explained by the conjoint influence from ROI 1. Despite its utility, this statistical approach is often challenging to apply in small samples (which is particularly the case of the VBM data in this study). In any dataset $\chi \in \mathbb{R}^{n \times p}$, considerable estimation errors can

arise when the number of unknown model parameters exceeds the number of samples by $n < \frac{1}{2} p(p+1)$.

To overcome erroneous eigenstructure, statistical conditioning was improved by imposing sparsity assumptions by means of ℓ_1 penalization (Figure 2c) of the inverse covariance estimation (Friedman et al., 2008; Hastie, Tibshirani, & Wainwright, 2015). In the case of multivariate Gaussian models, conditional independence between ROIs is given by the zero entries in the precision (i.e., inverse covariance) matrix. Incorporating this frequentist prior automatically reduces the model complexity by identifying the most important pairs of network nodes and ignoring the remainder. In the case of graphs, selecting those covariance parameters in the space of possible covariance models with sparse support (i.e., several zero-valued parameters in the graph) equates to limiting the number of graph edges. This sparse model estimation automatically balances the compromise between biasing towards model simplicity (hence, neurobiological interpretability) and obtaining optimal model fits to brain data. The degree of ℓ_1 penalization, controlled by the coefficient λ , was evaluated and selected in the cross-validation procedure. One important consequence of ℓ_1 penalization is that searching the covariance structure reduces to a convex problem with a unique solution. Hence, rerunning the sparse inverse covariance estimation with different random initializations of the model parameters will yield an identical solution each time.

In sum, detailed probabilistic models of network coupling were automatically derived from multisite brain data by using sparse inverse covariance estimation in both groups (i.e., healthy subjects and patients with schizophrenia). Models derived from RSFC data could be interpreted as summarizing the most important functional connections, while models derived from VBM data could be interpreted as summarizing the most important volumetric co-occurrences.

2.6 | Testing for significant disturbance in DMN covariation

Sparse inverse covariance estimation based on RSFC and separately on VBM was to be conducted separately in the healthy group and the group of patients with schizophrenia. Separate precision matrices were thus obtained in normal controls and people with schizophrenia. Statistical significance for group differences (Figure 2d) was assessed based on (family wise error, multiple-comparison corrected) p -values for the multivariate DMN covariation based on bootstrapping for nonparametric hypothesis testing (Miller et al., 2016; Smith et al., 2015). A series of bootstrap samples ($n = 1,000$) were drawn with replacement from the healthy brain data (i.e., RSFC data for functional connectivity and VBM data for the volumetric co-occurrence). For each of the thus generated 1,000 alternative dataset realizations, we performed all above steps of the sparse inverse covariance estimation (Efron & Tibshirani, 1994). This computation generated a null distribution of possible covariation estimates for every ROI-ROI relation in healthy individuals. Bootstrapping thus provided interval estimates that indicated how each coupling strength of the DMN was expected to vary in the general population (Hastie, Tibshirani, & Friedman, 2001).

Statistically significant differences between the healthy group and the group of patients with schizophrenia were then tested at the threshold corresponding to $p < 0.001$ by assessing whether the true coupling strength in individuals with schizophrenia was higher or lower than 99.9% of the coupling strengths in the healthy population. Note that, in VBM data, we have applied a more lenient threshold corresponding to $p < 0.05$, which led to statistical significance when structural covariation in schizophrenia exceeded the healthy distribution in 95% of the bootstrap samples. This is because the VBM analyses were performed in a small-sample scenario (i.e., as many brain images as participants), whereas the RSFC analyses were performed in a large-sample scenario (i.e., tens of thousands of brain images). In so doing significance testing for group differences, first in the functional covariation and then in the structural covariation, has been explicitly corrected for multiple testing, searching across all ROI pairs estimated (Miller et al., 2016; Smith et al., 2015).

3 | RESULTS

3.1 | Impact of studying nodes versus subnodes in the DMN

Based on brain measurements of functional connectivity (i.e., RSFC) in one set of analyses and structural co-occurrence (i.e., VBM) in another set of analyses, we initially examined whether subdividing traditionally studied DMN nodes into subnodes would provide richer information in brain signals. Based on 4 DMN nodes (Figure 1a) versus 12 DMN subnodes (Figure 1b), we therefore computed sparse inverse covariance estimates (i.e., precision matrices) and their statistically significant group differences (Figure 2).

In brain function as measured by RSFC, only the functional covariation between the right and the left TPJ of the DMN was determined to be significantly different between the healthy control and people with schizophrenia (Figure 3a). We then enhanced topographical granularity. Dividing the main nodes of the DMN into their constituent subnodes confirmed the observed effect (Figure 3b). We further observed that significant aberration did not involve the functional connectivity between the left anterior TPJ (aTPJ) and right posterior TPJ (pTPJ) subnodes. Importantly, a number of additional significant effects were not captured by the subnode-naïve connectivity analyses of the DMN.

In brain structure as measured by VBM, only the structural covariation between the PMC and the left TPJ node was significantly different between the control and disease groups (Figure 3c). Segmenting the composite DMN nodes into their distinct subnodes revealed that the observed effect could be more specifically credited to the morphological coupling between the left aTPJ and the precuneus (PREC) subnodes (Figure 3d). Once more, a number of additional differences in structural covariation were observed.

These preparatory analyses converged to the conclusion that neurobiologically meaningful information contained in fMRI and MRI signals is likely to remain hidden when using a general-purpose atlas to define the human DMN. Adopting a more fine-grained subnode atlas allowed detailing previously shown and discovered new covariation

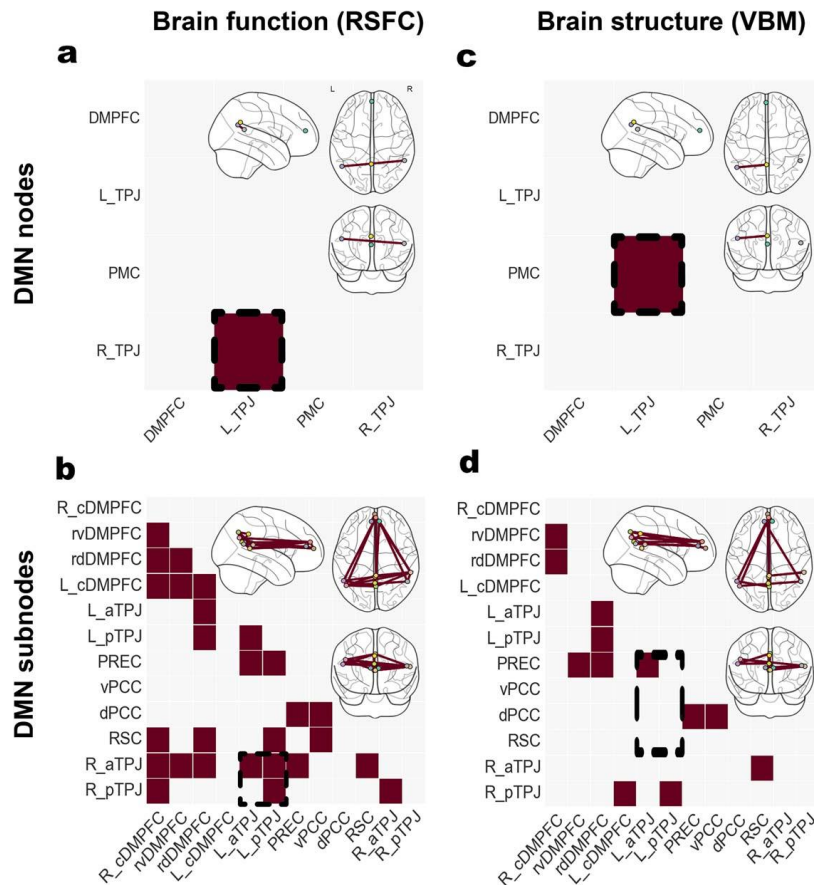


FIGURE 3 Studying nodes versus subnodes in the DMN. Significant differences in functional connectivity (left column, RSFC) and structural co-occurrence (right column, VBM). Schizophrenic patients and healthy controls were compared based on the usual DMN nodes (upper row) and the topographically more fine-grained DMN subnode atlas (lower row). Richer brain signals have been captured by the recent parcellation of the DMN nodes, resulting in a higher number of statistically significant group effects. Analysis approaches based on collapsed DMN nodes may therefore obfuscate disease-specific patterns in fMRI signals as indexed by resting-state connectivity and in MRI signals as indexed by VBM. The glass brains were created using the nilearn Python package (Abraham et al., 2014).

effects in the DMN. This observation held true for both assessing functional coupling patterns (i.e., RSFC) and structural coupling patterns (i.e., VBM) in the DMN. Consequently, the remainder of the results section will focus on statistical analyses based on DMN subnodes.

The subsequent functional and structural covariation analyses were performed in two complementary flavors. Intra-network analyses performed sparse inverse covariance estimation based on the 12 subnodes from the DMN atlas (Figure 1b). Across-network analyses performed the same multivariate modeling of network coupling but extended the 12 DMN subnodes with nine nodes from the DAN and the SN, which are two multimodal networks known to closely interact with the DMN (Figure 1c). Hence, intra-network analyses exposed the

coupling differences in the DMN between healthy controls and people with schizophrenia at the subnode level. This work was extended in across-network analyses to characterize the interplay between the DMN and two other multimodal large-scale networks.

3.2 | Intranetwork covariation in brain function

We systematically detailed the neural coupling fluctuations within the DMN in people with schizophrenia and healthy controls during the resting-state (i.e., RSFC). The functional intra-network analyses (Figure 5 and Supporting Information Fig. S1 upper row) revealed the right aTPJ as the subnode with the highest number of significantly disrupted

functional connections in the DMN. Eight out of 11 connectivity targets of the right aTPJ were disturbed, including connections to three subnodes in the DMPFC, the right pTPJ, both subnodes in the left TPJ, as well as the PREC and the RSC. The subnode with the second highest number of functional disturbances was the rostro-dorsal DMPFC (rdDMPFC) subnode. Seven out of 11 of its connection targets were significantly affected in people with schizophrenia including the right and left caudal DMPFC (cDMPFC), the rostro-ventral DMPFC (rvDMPFC), the RSC subnode as well as both subnodes in the left TPJ and the right aTPJ. Further, the right cDMPFC and the left pTPJ subnodes in the DMN exhibited 6 out of 11 affected connections. Both shared common aberrations to the RSC, to the rdDMPFC, and to the two right TPJs as connectivity targets. Conversely, the ventral and dorsal posterior cingulate cortex (vPCC and dPCC) in the DMN showed only 2 out of 11 significantly altered functional connections to other DMN subnodes. Both were restricted to connectivity targets in the PMC.

Regarding the direction of aberrant functional coupling, the right aTPJ was hyperconnected with the left TPJs and the rvDMPFC, while it was hypoconnected toward the RSC, PREC, rdDMPFC, and left pTPJ. DMPFC subnodes were hypoconnected with each other in patients compared to the healthy group. A set of further hypoconnections were observed involving significant aberrations of the right pTPJ and the PREC with other subnodes.

In sum, multivariate connectivity analyses based on functional resting-state fluctuations illustrated statistically significant disturbances in 27 out of 60 connections between subnodes of the DMN in patients with schizophrenia. Among these, the right aTPJ exhibited the highest and the vPCC and dPCC the lowest number of affected coupling strengths with other parts of the DMN.

3.3 | Across-network covariation in brain function

We then tested for group differences in the functional coupling between the DMN and the multimodal networks DAN and SN (Figures 4a and 5 and Supporting Information Fig. S1, second row). Importantly, after adding the nodes from the other two macroscopic brain networks for computing precision matrices, the overall pattern of covariation remained similar. In the intranetwork versus across-network analyses, the differences in functional covariation between DMN subnodes were not statistically significant at $p < 0.05$ (dependent t-test). These observations support the notion that the functional connectivity patterns delineated by sparse inverse covariance estimation on RSFC data are relatively robust to changes in the size and definition of the network graph (i.e., which nodes are included).

Regarding the DAN, the left IPS displayed the highest number of edges that were significantly disturbed in patients. Nine out of 20 connectivity targets were affected. These included six subnodes in the DMN (rdDMPFC, dPCC, both left TPJs, right aTPJ, and PREC) and nodes in the other two networks including the mid-cingulate cortex (MCC), the right AM and the right IPS. The left DLPFC in the DAN also showed disrupted connectivity with 8 out of 20 targets. These included six DMN subnodes (right cDMPFC, rvDMPFC, rdDMPFC, RSC, and both left TPJs) as well as nodes of the SN including the left AI and

MCC. The right IPS, in turn, showed seven affected connections, including DMN subnodes (rdDMPFC, left aTPJ, both right TPJs, PREC) and DAN nodes (left IPS and right DLPFC), but no part of the SN. Similar to its left-hemisphere counterpart, the right DLPFC showed six affected connections, including nodes of the SN (MCC, right AI), only one node of the DAN (right IPS), as well as several DMN subnodes (rdDMPFC, both left TPJs).

Regarding the SN, the MCC displayed 6 out of 20 functional connections disturbed in schizophrenia patients, including several DMN subnodes (left and right cDMPFC, and RSC) and nearly the entire DAN (left and right DLPFC, left IPS), but no other part of the SN. The left AI was the second most affected node with four aberrant connections, including only one DMN subnode (left cDMPFC), one DAN node (left DLPFC), and two SN nodes (right AI, left AM). The right AM in turn showed only three affected connections with the DMN (right cDMPFC, RSC) and DAN (left IPS). The right AI showed three affected connections with the DMN (dPCC), the DAN (right DLPFC), and the SN (left AI). Finally, the left AM had only two affected connections with the DMN (rvDMPFC) and the SN (left AI). As a general observation, the highest number of functional disruptions therefore appeared between the DMN and the DAN.

Regarding the directionality of functional coupling aberration, the right DLPFC of the DAN was hypoconnected with the DMN, whereas the left DLPFC and the default network were hyperconnected except with the rdDMPFC. As a similar pattern, the right IPS of the DAN was mostly hypoconnected with the DMN, except with the left aTPJ, while the left IPS was mostly hyperconnected except with the left pTPJ and the PREC. As to the SN, only the MCC and the right AM exhibited hypoconnectivities with the DMN, with the right cDMPFC and the RSC, respectively.

Summing up the present findings in functional connectivity data within and from the DMN, we made several observations. First, the right aTPJ emerged as a potential driver of perturbations to network coupling observed in schizophrenia, especially when focusing on functional covariation within the DMN (i.e., intranetwork analysis). Importantly, this subnode of the DMN has been repeatedly reported not to be part of the functional core of this canonical network (Bzdok et al., 2013; Mars et al., 2012). Second, many of the subnodes, here identified to drive dysfunction in schizophrenia, are not part of what is emerging to be a default-mode network proper. According to previous studies, such a stricter topographical definition of the DMN core does most likely not include the left and right anterior TPJs, the PREC (Bzdok et al., 2015; Margulies et al., 2009), the left and right cDMPFC (Eickhoff et al., 2016), or the RSC (Bzdok et al., 2015). Indeed, parts of the DMN core, the vPCC and dPCC, were among the least dysfunctional target regions in both intra- and across-network analyses. Third, the functional abnormalities in schizophrenia frequently manifested between commonly observed macroscopic networks, especially between the DMN and the DAN.

3.4 | Intranetwork covariation in brain structure

We conducted an analysis in the domain of brain structure using the VBM data that was analogous to the assessments of brain function.

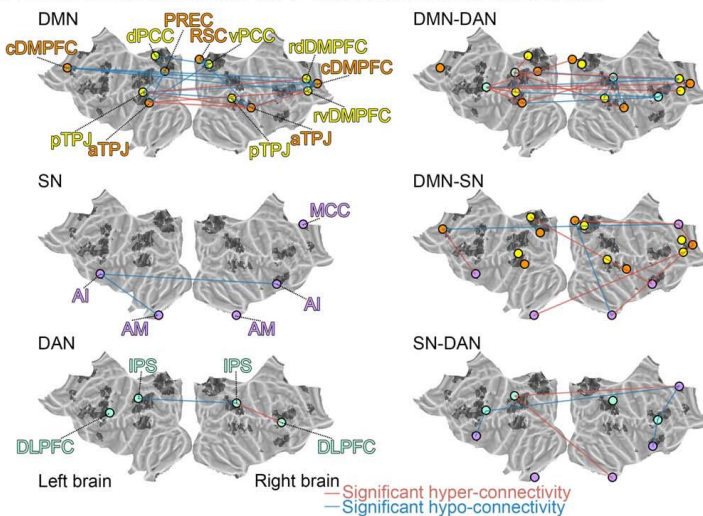
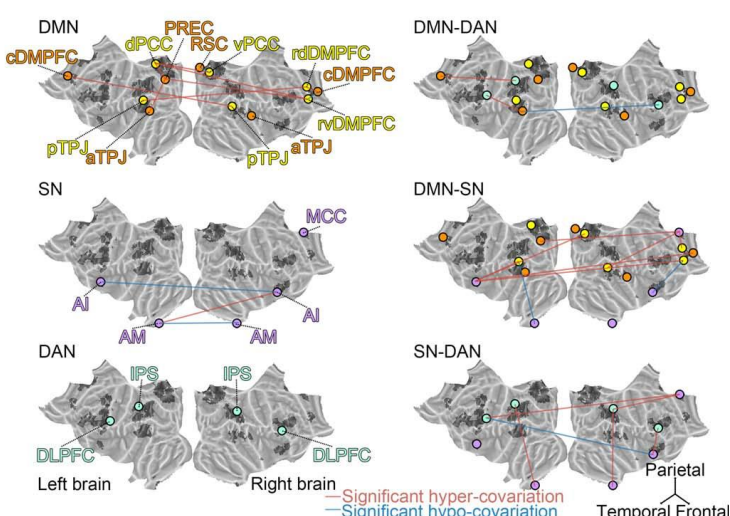
a. DYSFUNCTIONAL HYPER- AND HYPO- CONNECTIVITY ACROSS NETWORKS**b. ABERRANT STRUCTURAL HYPER- AND HYPO- COVARIATION ACROSS NETWORKS**

FIGURE 4 Dysfunctional connectivity and aberrant structural covariation across networks. Depicts the significant increase (red lines) or decrease (blue lines) in functional connectivity (a) or in structural co-occurrence (b) comparing schizophrenic to healthy subjects in the across-network RSFC analyses (cf. Supporting Information Fig. S1). Circles represent regions of interest in the DMN (orange), the "DMN proper" (yellow), the SN (purple), and the DAN (light green). The left column shows the differences within each network, while the right column displays differences between two networks. The connectivity findings show that the dysfunctional connectivities within the DMN include several subnodes that are not part of the "DMN proper." While the functional coupling between the DMN and the SN is partly disrupted, the functional connectivity between the DMN and the DAN is particularly disturbed. Furthermore, the connectivities within and between the SN and the DAN remain largely intact. The covariance findings show that the deviant structural covariations within the DMN involve several subnodes not part of the "DMN proper." The volumetric relationships between the DMN and the SN are also more disrupted than between any other network pair. Collectively, the findings emphasize internetwork dysregulation rather than exclusive disturbance of the DMN core parts. Flat brains were generated using PyCortex (Gao, Huth, Lescroart, & Gallant, 2015).

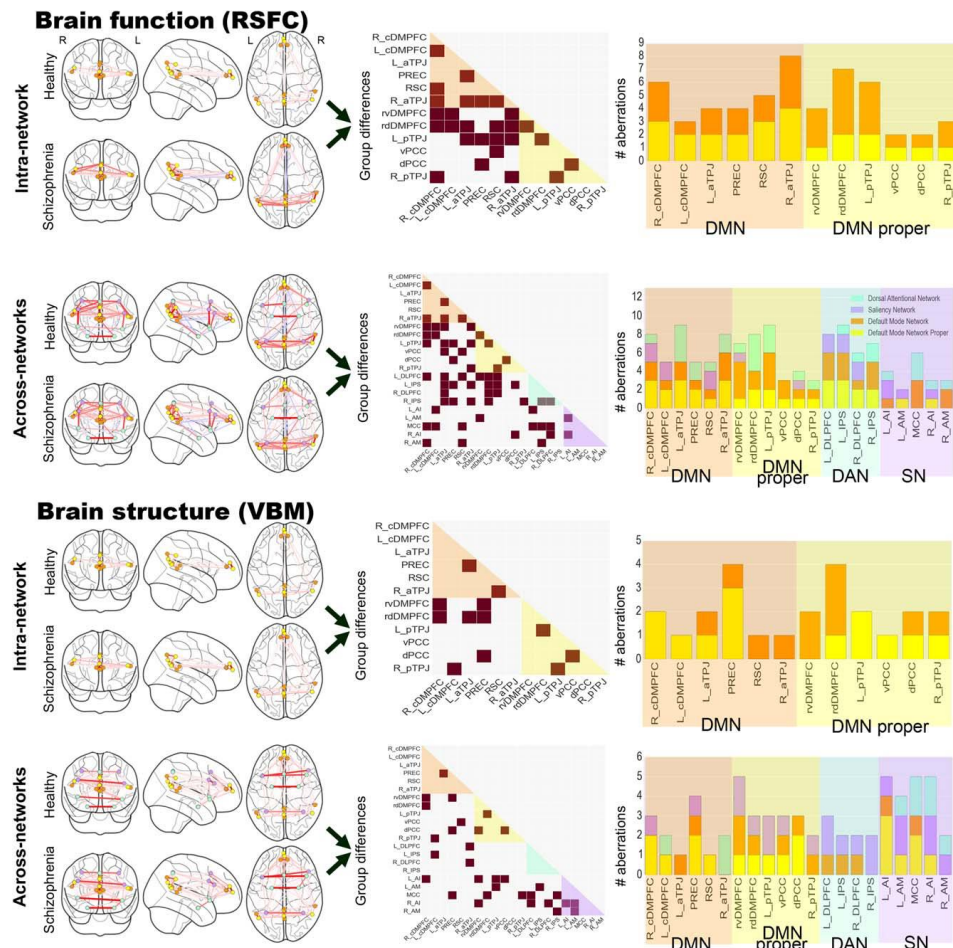


FIGURE 5 DMN aberrations in schizophrenia are specific to subnodes. Functional connectivity (RSFC) and structural co-occurrence (VBM) measurements were used to compute sparse inverse covariance estimation separately in healthy and schizophrenic individuals (left column). We conducted intra-network analyses (i.e., DMN subnode atlas) and across-network analyses (i.e., DMN subnode atlas augmented by nodes of the DAN and SN). Statistically significant group differences (brown squares in middle column) between the normal and diagnosed individuals are shown as derived from sparse inverse covariance estimation. The number of subnode-specific dysregulations (right column) is shown as counts when viewed from the DMN proper (yellow), other DMN parts (orange), DAN (light green), and SN (purple). The findings make apparent that schizophrenia pathophysiology may be relatively more driven by across-network effects and effects outside of the DMN proper. The glass brains were created using the nilearn Python package (Abraham et al., 2014)

We thus investigated the inter-individual morphological variability within the DMN in healthy subjects and patient with schizophrenia. The structural co-occurrence results from covariation analyses on VBM data were then also evaluated for statistically significant group differences.

The structural intra-network analyses (Figure 5 and Supporting Information Fig. S1, third row) revealed DMN subnodes in the PREC and the rdDMPFC as the target regions with highest structural

disturbances in people with schizophrenia. For the PREC, 4 out of 11 volumetric co-occurrence relations were affected, including the medial frontal pole (rvDMPFC and rdDMPFC), dPCC, and left aTPJ. The rdDMPFC in turn showed four affected volumetric relations, including the right cDMPFC, both left TPJ subnodes, and the PREC. Conversely, only a single disturbed structural relation with other parts of the DMN was found for the right aTPJ, left cDMPFC, vPCC, and RSC.

The large majority of structural coupling aberrations were hypercovariations between DMN subnodes. Specifically, all PMC subnodes, including the PREC, both pTPJs, the right aTPJ and cDMPFC exhibited only hypercovariations. Further, the left aTPJ was hypoconnected with the rdDMPFC and the right cDMPFC was hypoconnected with the rvDMPFC.

In sum, the intranetwork analyses of structural co-occurrence illustrated that the DMN subnode atlas was instrumental in identifying fine-grained differences in morphological deviations in a large group of people diagnosed as schizophrenic. Healthy and diagnosed subjects showed statistically significant differences in a fifth of the volumetric coupling relations within the DMN (12 out of 60). This result stands in contrast to the higher number of functional aberrations found in the corresponding analyses in the functional imaging arm of the study (RSFC).

3.5 | Across-network covariation in brain structure

We finally tested for group differences in structural covariation between the DMN and the DAN and SN (Figures 4b and 5 and Supporting Information Fig. S1, lowest row). Concurrent with the functional covariation analyses, the overall pattern of structural coupling was similar when computing the precision matrices after taking into account the nodes of the DAN and SN. In the intranetwork versus across-network analyses, the differences in structural covariation between DMN subnodes were not statistically significant at $p < 0.05$ (dependent t-test). As another global observation, none of the structural analyses showed any negative covariation in the healthy or disease group, in contrast to the various positive and negative coupling results observed in the functional covariation analyses. Moreover, we again showed a lower overall number of statistically significant volume differences in people with schizophrenia (31 significant abnormalities) compared with the corresponding group differences in brain function (61 significant abnormalities).

Regarding the DAN, we identified the left DLPFC as exhibiting statistically significant differences between healthy controls and people with schizophrenia in 3 out of 20 volumetric relations. These included the right aTPJ, MCC, and right AI. Congruently, the DLPFC in the right hemisphere also exhibited affected volumetric relations with the right aTPJ and the right AI. Further, the right and left IPS both showed impaired volumetric coupling with the AM of the same hemisphere. While the right IPS was also disrupted in its volumetric relation with the MCC, the left IPS displayed another impaired relation with the left cDMPFC.

Regarding the SN, the MCC as well as left and right AI of this same commonly observed multimodal network showed the highest number of impaired volumetric couplings (besides rvDMPFC). All three SN nodes showed disturbed relations with subnodes in the DMPFC. More specifically, left AI exhibited four affected relations, including the right cDMPFC, the rvDMPFC, the vPCC, the left pTPJ, and the right AI. The AI in the right hemisphere instead showed affected relations with rvDMPFC, left AI, left AM, as well as the right and left DLPFC. The MCC had five affected volumetric relations including the rdDMPFC,

the PREC, the left DLPFC, as well as the IPS and pTPJ in the right hemisphere. Finally, both AM showed dysfunctional structural coupling among each other as well as to the IPS in the same hemisphere, while the left AM showed additional abnormalities with the right AI and the left pTPJ. As a general observation, the highest number of structural disruptions emerged between the DMN and the SN.

Consistent with the intranetwork analysis in brain structure, patients mostly exhibited significant hypercovariations between the DMN and the other canonical networks. Specifically, both the MCC and the right AI, the most disrupted SN nodes towards the DMN, exhibited only hypercovariations while the SN exhibited hypcovariations with the DMN only from the left AM and the right AI.

In sum, major brain networks, such as the DAN and SN, demonstrated specific volumetric coupling relations with distinct subnodes of the DMN that were shown to be impaired in schizophrenia. Importantly, only a few subnodes of the DMN proper showed statistically significant group differences. Similar to the present finding in brain function, the morphological properties of the DMN proper were found to be more intact than many other parts of the graph. Moreover, nodes of the SN were most impaired among all three networks and featured most aberrations with coupling partners of the DMN proper.

4 | DISCUSSION

Our study suggests that disconnectivity and dysregulation anchored in the DMN is a neurobiological hallmark of schizophrenia spectrum disorders. Adopting a systems neuroscience approach, we aimed at reconciling coupling within the highly associative DMN and its coupling with the multimodal saliency and dorsal attention networks. We combined meta-analytically defensible network definitions and recently developed machine learning methods for multivariate discovery of primary covariation patterns. Network coupling was investigated in two domains, first, based on brain measurements of functional resting-state fluctuations (i.e., RSFC) and second, based on structural brain morphology (i.e., VBM). Applying an identical modeling strategy to observed functional fluctuations and volumetric differences facilitated conclusions across neurobiological levels, including their third-party coupling influences. Functional covariation analyses revealed extended disturbances related to the right anterior TPJ and the DAN. In contrast, structural covariation analyses emphasized disturbances related to the precuneus in the PMC and the SN. These findings emphasize disturbed coupling between the DMN and other large-scale networks rather than exclusive dysregulation of core parts within the DMN. Collectively, our results suggest that some previously inconsistent findings may be reconciled by using a DMN atlas with subnode resolution to recover currently under-appreciated, physiologically meaningful covariation patterns in schizophrenia.

4.1 | Covariation patterns mostly altered by cortical areas that are not part of the “DMN proper”

Covariation analyses applied to resting-state fluctuations within and from the DMN identified the right anterior TPJ subnode as featuring a

particularly high number of coupling perturbations in people diagnosed as schizophrenic, especially in the functional intranetwork analyses. Recent brain parcellation studies have associated the anterior portions of the TPJs with externally focused evaluation of visual, auditory, tactile, and other preprocessed sensory input as well as maintenance of perception-action cycles associated with the SN (Bzdok et al., 2013, 2016a; Glasser et al., 2015; Humphreys & Ralph, 2015; Mars et al., 2012). Hence, this investigation at subnode granularity points to an aberration of multimodal integration of perception-action cycles, more closely linked to DAN and SN function, rather than to imagination-based thought processes, more closely linked to DMN function (Hassabis, Kumaran, & Maguire, 2007; Wang et al., 2017). This quantitative evidence potentially relates to several clinical manifestations of schizophrenia, such as false subjective beliefs (delusion), perceiving unreal stimuli (hallucinations), awkward sensations (paresesthesia), concentration difficulties, as well as disorganized speech and motor movement.

Across structural covariation analyses, the PREC emerged as one of the most impaired DMN nodes. The PREC is anatomically located in the parietal lobe and is thought to subserve visuomotor processes, such as those necessary for attentional shifting, reaching movements, and hand-eye coordination (Margulies et al., 2009; Mesulam, 1981; Stephan et al., 1995). These cognitive associations ascribed to the PREC can indeed be related to several schizophrenia symptoms, especially loss of train of thought, impairments in executive function, working memory, and memory retrieval, as well as psychogenic motor abnormalities (catatonia). Both anterior TPJs and the PREC are similarly believed to govern context-dependent reorganization of large-scale networks (Bzdok et al., 2013; Cavanna & Trimble, 2006; Downar, Crawley, Mikulis, & Davis, 2000; Seghier, 2013).

As a general conclusion, functional and structural findings agreed in emphasizing that (i) the communication within the medial core of the DMN in prefrontal and cingulate regions was relatively preserved in the examined patients and (ii) the dysfunction of schizophrenia substantially involves subnodes that do not belong to what is emerging to be a default mode network proper. Such a stricter topographical definition of the DMN excludes the anterior left and right TPJ, the PREC (Bzdok et al., 2015; Margulies et al., 2009), the RSC closer to the limbic system (Braga & Buckner, 2017; Bzdok et al., 2015; Vogt & Laureys, 2005), and the caudal DMPFCs closer to the anterior cingulate cortex (Eickhoff et al., 2016; Vogt & Pandya, 1987). Instead, our definition of the DMN core includes the ventral and the dorsal PCCs, the left and right posterior TPJs, and the rostralventral and rostrodorsal DMPFC. Both the ventral and dorsal PCCs were identified among the least dysfunctional areas across all present analyses.

Collectively, these data suggest that dysfunctions in the DMN that underpin schizophrenia pathology do not emerge from the core of the network, but are reflected in the coupling of the subnodes of the larger network, regions that prior work has implicated as participating in large-scale networks other than the DMN. In particular, our study highlights disturbed internetwork communication, focused on the right anterior TPJ and PREC, as candidate drivers of the disease process that underpins schizophrenia.

4.2 | Discrepancies between volumetric and functional aberration patterns in schizophrenia

In the context of schizophrenia, network analyses have frequently been performed on either functional brain measurements (Liu et al., 2008; Lynall et al., 2010; Yu, Sui, Kiehl, Pearson, & Calhoun, 2013) or structural brain measurements (Konrad & Winterer, 2008; van den Heuvel, Mandl, Stam, Kahn, & Pol, 2010). Direct investigations of the volume-function correspondence in long-distance coupling have been less frequent (But see: Clos, Rottschy, Laird, Fox, & Eickhoff, 2014; Honey et al., 2009; Kelly et al., 2012).

This study departs from previous single-modality investigations by applying identical covariation analyses to RSFC and VBM data to facilitate neurobiological conclusions independent of differences in the employed statistical models. We did not find strong evidence that these neurobiological domains show analogous patterns when considering the DMN in isolation or its interplay with the DAN and SN. In the functional domain, for instance, the right anterior TPJ was the overall most affected subnode, while the PREC and the right dorsal DMPFC exhibited the strongest disruptions in the structural domain. These findings suggest that neural disturbances in schizophrenia are a result of heterogeneous changes in cortex architecture that do not map in a simple way to patterns of neural communication. In addition, these regularities emphasize abnormalities in schizophrenia between networks rather than within the DMN core.

Given that the DMN is believed to exert control over the subordinate DAN and SN (Carhart-Harris & Friston, 2010; Margulies et al., 2016), it is exciting that our results revealed a dissociation in their disrupted links in the structural and functional network analyses. DMN interactions with the SN were more consistently altered in brain morphology (VBM), whereas DMN interactions with the DAN emerged as more consistently altered in brain function (RSFC) in patients with schizophrenia. Congruently, previous quantitative meta-analysis on schizophrenia and other psychiatric populations highlighted aberration in the SN across volumetric neuroimaging studies (Goodkind et al., 2015) and dysfunction in the DAN in large amounts of functional neuroimaging studies (McTeague et al., 2017). Both inter-individual differences in local brain volume (e.g., Draganski et al., 2004) and fluctuations in resting-state patterns (e.g., Rosenberg et al., 2015) have been shown to offer reliable correlates of success and failure in specific cognitive performances (Kanai & Rees, 2011). Differences in the executive control performance between healthy individuals were related to cortical thickness differences in the SN extending into parts of the DMN (Westlye, Grydeland, Walhovd, & Fjell, 2011). The present pathological increases in structural DMN-SN coupling may therefore provide insight into a longer-term compensatory mechanism due to impaired executive function in patients with schizophrenia. In contrast, the present patterns of pathological increases and decreases in functional DMN-DAN coupling may uncover a multifaceted dysbalance in allocating attentional resources to internal thought and emotion (cf. Shim et al., 2010; Whitfield-Gabrieli et al., 2009). Thus, previous isolated findings are reconciled by our integrative analysis pipeline that situated detailed disruption patterns in the context of top-level DMN control on intermediate multimodal networks.

Although we did not find a close mapping between structure and function, in both domains we found evidence that corroborates the disconnection hypothesis of schizophrenia (Friston et al., 2016; Friston & Frith, 1995; Stephan et al., 2009; Weinberger et al., 1992) as a central pathophysiological component that could underlie schizophrenia spectrum disorders. Together, our findings support an account of the pathophysiology of schizophrenia in which abnormal integrity of long-range connections prevent integration of information from systems that support the maintenance of cognitive sets, such as mediated by the SN, or the dynamic allocation of cognitive resources, such as mediated by the DAN (Dosenbach et al., 2006; Seeley et al., 2007).

4.3 | Future directions

More globally, the overwhelming majority of mental disorders are known to show some disturbance of the DMN (Broyd et al., 2009; Whitfield-Gabrieli & Ford, 2012). Yet, we deem it unlikely that brain disorders with diverging clinical phenotypes are caused by identical neurobiological disease mechanisms. Rather, the numerous brain disorders affecting the DMN are perhaps more realistically framed to underlie a stratification of partly overlapping pathophysiologies (cf. Calhoun et al., 2011; Meda et al., 2012; Öngür et al., 2010). Investigating the DMN at an increased level of topographic granularity may be a prerequisite for identifying the DMN dysregulation specific to each major psychiatric disorder. A variety of neurobiologically distinct types of DMN aberration may expose brain phenotypes that enable effective stratification of patients with schizophrenia in clinical practice (Brodersen et al., 2011). If successful in schizophrenia, this analysis framework may scale to other major psychiatric disorders.

Moreover, our approach leveraging sparse inverse covariance estimation has several advantages, including enhanced interpretability, statistically privileging direct network influences, and interoperability across different brain-imaging modalities. However, the employed statistical model is inherently blind to interaction partners outside of the network graph and disregards higher-order interaction between the nodes in the network graph (Ganmor, Segev, & Schneidman, 2011; Giusti, Ghrist, & Bassett, 2016; Giusti, Pastalkova, Curto, & Itskov, 2015). That is, our analysis strategy was able to consider all targeted intermodal relations simultaneously but assumed network interaction to be only composed of a set of dyadic partners. Going beyond pair-wise covariation in network analysis would be an exciting future extension of this work (Bassett & Sporns, 2017).

5 | CONCLUSION

Conventional brain-imaging measurements of the highly associative DMN were shown to carry fine-grained information about its coupling relation to other macroscopic brain networks. We could thus conclude that schizophrenia may not be explained by a primary dysfunction in the backbone of the DMN ("default mode network proper"). Schizophrenia psychopathology may not only be due to deficits within the DMN but especially also to deficits between the DMN and other multimodal networks including the SN and DAN. Further, by leveraging

state-of-the-art machine learning techniques for a direct juxtaposition of functional and structural covariation patterns, we provide empirical evidence for complementary disease mechanisms in schizophrenia patients. These first steps towards a more integrative approach to study DMN disturbance may be critical to chisel out the "disconnection" pathophysiology potentially underlying schizophrenia.

ACKNOWLEDGMENTS

Dr. Bzdok is funded by the Deutsche Forschungsgemeinschaft (DFG, BZ2/2-1, BZ2/3-1, and BZ2/4-1; International Research Training Group IRTG2150), Amazon AWS Research Grant (2016 and 2017), the German National Merit Foundation, and the START-Program of the Faculty of Medicine, RWTH Aachen. Dr. Bassett acknowledges support from the John D. and Catherine T. MacArthur Foundation, the Alfred P. Sloan Foundation, the Army Research Laboratory and the Army Research Office through contract numbers W911NF-10-2-0022 and W911NF-14-1-0679, the National Institute of Mental Health (2R01-DC-009209-11), the National Institute of Child Health and Human Development (1R01HD086888-01), the Office of Naval Research, and the National Science Foundation (BCS-1441502, BCS-1430087, NSF PHY-1554488). Dr. Margulies and Dr. Smallwood received support from the Wellcome Trust 103817/Z/14/Z and from the Volkswagen Foundation (Wandering Minds – 89440 and 89439). Dr. Smallwood was further supported by the European Research Council (WANDERGMINDS–646927).

ORCID

Jérémie Lefort-Besnard  <http://orcid.org/0000-0002-8033-4953>
 Danielle S. Bassett  <http://orcid.org/0000-0002-6183-4493>
 Bertrand Thirion  <http://orcid.org/0000-0001-5018-7895>

REFERENCES

- Abraham, A., Pedregosa, F., Eickenberg, M., Gervais, P., Mueller, A., Kosaiifi, J., ... Varoquaux, G. (2014). Machine learning for neuroimaging with scikit-learn. *Frontiers in Neuroinformatics*, 8, 14.
- Andrews-Hanna, J. R., Reidler, J. S., Sepulcre, J., Poulin, R., & Buckner, R. L. (2010). Functional-anatomic fractionation of the brain's default network. *Neuron*, 65(4), 550–562.
- Andrews-Hanna, J. R., Smallwood, J., & Spreng, R. N. (2014). The default network and self-generated thought: Component processes, dynamic control, and clinical relevance. *Annals of the New York Academy of Sciences*, 1316(1), 29–52.
- Ashburner, J., & Friston, K. J. (2005). Unified segmentation. *Neuroimage*, 26(3), 839–851.
- Bado, P., Engel, A., Oliveira- Souza, R., Bramati, I. E., Paiva, F. F., Basilio, R., ... Moll, J. (2014). Functional dissociation of ventral frontal and dorsomedial default mode network components during resting state and emotional autobiographical recall. *Human Brain Mapping*, 35(7), 3302–3313.
- Bassett, D. S., & Sporns, O. (2017). Network neuroscience. *Nature Neuroscience*, 20(3), 353–364.
- Behrens, T. E., Johansen-Berg, H., Woolrich, M. W., Smith, S. M., Wheeler-Kingshott, C. A., Boulby, P. A., ... Matthews, P. M. (2003).

- Non-invasive mapping of connections between human thalamus and cortex using diffusion imaging. *Nature Neuroscience*, 6(7), 750–757.
- Bluhm, R. L., Miller, J., Lanius, R. A., Osuch, E. A., Boksmann, K., Neufeld, R. W. J., ... Williamson, P. (2007). Spontaneous low-frequency fluctuations in the BOLD signal in schizophrenic patients: Anomalies in the default network. *Schizophrenia Bulletin*, 33(4), 1004–1012.
- Braga, R. M., & Buckner, R. L. (2017). Parallel interdigitated distributed networks within the individual estimated by intrinsic functional connectivity. *Neuron*, 95(2), 457–471.e5.
- Brodersen, K. H., Schofield, T. M., Leff, A. P., Ong, C. S., Lomakina, E. I., Buhmann, J. M., & Stephan, K. E. (2011). Generative embedding for model-based classification of fMRI data. *PLoS Computational Biology*, 7(6), e1002079.
- Broyd, S. J., Demaneule, C., Debener, S., Helps, S. K., James, C. J., & Sonuga-Barke, E. J. (2009). Default-mode brain dysfunction in mental disorders: a systematic review. *Neuroscience and Biobehavioral Reviews*, 33(3), 279–296.
- Buckner, R. L., Andrews-Hanna, J. R., & Schacter, D. L. (2008). The brain's default network. *Annals of the New York Academy of Sciences*, 1124(1), 1–38.
- Buckner, R. L., & Krienen, F. M. (2013). The evolution of distributed association networks in the human brain. *Trends in Cognitive Sciences*, 17(12), 648–665.
- Bzdok, D., Hartwigsen, G., Reid, A., Laird, A. R., Fox, P. T., & Eickhoff, S. B. (2016a). Left inferior parietal lobe engagement in social cognition and language. *Neuroscience and Biobehavioral Reviews*, 68, 319–334.
- Bzdok, D., Heeger, A., Langner, R., Laird, A. R., Fox, P. T., Palomero-Gallagher, N., ... Eickhoff, S. B. (2015). Subspecialization in the human posterior medial cortex. *Neuroimage*, 106, 55–71.
- Bzdok, D., Langner, R., Schilbach, L., Jakobs, O., Roski, C., Caspers, S., ... Eickhoff, S. B. (2013). Characterization of the temporo-parietal junction by combining data-driven parcellation, complementary connectivity analyses, and functional decoding. *Neuroimage*, 81, 381–392.
- Bzdok, D., Schilbach, L., Vogeley, K., Schneider, K., Laird, A. R., Langner, R., & Eickhoff, S. B. (2012). Parsing the neural correlates of moral cognition: ALE meta-analysis on morality, theory of mind, and empathy. *Brain Structure & Function*, 217(4), 783–796.
- Bzdok, D., Varoufaux, G., Grisel, O., Eickenberg, M., Poupon, C., & Thirion, B. (2016b). Formal models of the network co-occurrence underlying mental operations. *PLoS Computational Biology*, 12(6), e1004994.
- Calhoun, V. D., Sui, J., Kiehl, K., Turner, J., Allen, E., & Pearlson, G. (2011). Exploring the psychosis functional connectome: Aberrant intrinsic networks in schizophrenia and bipolar disorder. *Frontiers in Psychiatry*, 2, 75.
- Camchong, J., Lim, K. O., Sponheim, S. R., & MacDonald, A. W. (2009). Frontal white matter integrity as an endophenotype for schizophrenia: Diffusion tensor imaging in monozygotic twins and patients' non-psychotic relatives. *Frontiers in Human Neuroscience*, 3, 35.
- Camchong, J., MacDonald, A. W., Bell, C., Mueller, B. A., & Lim, K. O. (2011). Altered functional and anatomical connectivity in schizophrenia. *Schizophrenia Bulletin*, 37(3), 640–650.
- Carhart-Harris, R. L., & Friston, K. J. (2010). The default-mode, ego-functions and free-energy: A neurobiological account of Freudian ideas. *Brain*, 133(Pt 4), 1265–1283.
- Cavanna, A. E., & Trimble, M. R. (2006). The precuneus: A review of its functional anatomy and behavioural correlates. *Brain: A Journal of Neurology*, 129(Pt 3), 564–583.
- Chai, X. J., Castanon, A. N., Ongur, D., & Whitfield-Gabrieli, S. (2012). Anticorrelations in resting state networks without global signal regression. *Neuroimage*, 59(2), 1420–1428.
- Clos, M., Rottschy, C., Laird, A. R., Fox, P. T., & Eickhoff, S. B. (2014). Comparison of structural covariance with functional connectivity approaches exemplified by an investigation of the left anterior insula. *Neuroimage*, 99, 269–280.
- D'Argembeau, A., Raffard, S., & Van der Linden, M. (2008). Remembering the past and imagining the future in schizophrenia. *Journal of Abnormal Psychology*, 117(1), 247.
- DeLisi, L. E. (2001). Speech disorder in schizophrenia: Review of the literature and exploration of its relation to the uniquely human capacity for language. *Schizophrenia Bulletin*, 27(3), 481.
- Dosenbach, N. U., Visscher, K. M., Palmer, E. D., Miezin, F. M., Wenger, K. K., Kang, H. C., ... Petersen, S. E. (2006). A core system for the implementation of task sets. *Neuron*, 50(5), 799–812.
- Downar, J., Crawley, A. P., Mikulis, D. J., & Davis, K. D. (2000). A multimodal cortical network for the detection of changes in the sensory environment. *Nature Neuroscience*, 3(3), 277–283.
- Draganski, B., Gaser, C., Busch, V., Schüller, G., Bogdahn, U., & May, A. (2004). Neuroplasticity: Changes in grey matter induced by training. *Nature*, 427(6972), 311–312.
- Du, Y., Pearson, G. D., Yu, Q., He, H., Lin, D., Sui, J., ... Calhoun, V. D. (2016). Interaction among subsystems within default mode network diminished in schizophrenia patients: A dynamic connectivity approach. *Schizophrenia Research*, 170(1), 55–65.
- Efron, B., & Tibshirani, R. J. (1994). *An introduction to the bootstrap*. New York: Chapman & Hall.
- Eickhoff, S. B., Laird, A. R., Fox, P. T., Bzdok, D., & Hensel, L. (2016). Functional Segregation of the Human Dorsomedial Prefrontal Cortex. *Cerebral Cortex (New York, N.Y.: 1991)*, 26(1), 304–321.
- Eickhoff, S. B., Thirion, B., Varoufaux, G., & Bzdok, D. (2015). Connectivity-based parcellation: Critique and implications. *Human Brain Mapping*, 36(12), 4771–4792.
- Fox, M. D., & Raichle, M. E. (2007). Spontaneous fluctuations in brain activity observed with functional magnetic resonance imaging. *Nature Reviews Neuroscience*, 8(9), 700–711.
- Friedman, J., Hastie, T., & Tibshirani, R. (2008). Sparse inverse covariance estimation with the graphical lasso. *Biostatistics (Oxford, England)*, 9 (3), 432–441.
- Friston, K., Brown, H. R., Siemerkus, J., & Stephan, K. E. (2016). The dysconnection hypothesis (2016). *Schizophrenia Research*, 176(2–3), 83–94.
- Friston, K. J., & Frith, C. D. (1995). Schizophrenia—a disconnection syndrome. *Clinical Neuroscience (New York, N.Y.)*, 3, 89–97.
- Frith, C. D., & Corcoran, R. (1996). Exploring 'theory of mind' in people with schizophrenia. *Psychological Medicine*, 26(03), 521–530.
- Gammie, E., Segev, R., & Schneiderman, E. (2011). Sparse low-order interaction network underlies a highly correlated and learnable neural population code. *Proceedings of the National Academy of Sciences of the United States of America*, 108(23), 9679–9684.
- Gao, J. S., Huth, A. G., Lescroart, M. D., & Gallant, J. L. (2015). Pycortex: An interactive surface visualizer for fMRI. *Frontiers in Neuroinformatics*, 9, 23.
- Garrity, A. G., Pearson, G. D., McKiernan, K., Lloyd, D., Kiehl, K. A., & Calhoun, V. D. (2007). Aberrant "default mode" functional connectivity in schizophrenia. *American Journal of Psychiatry*, 164(3), 450–457.
- Giusti, C., Ghris, R., & Bassett, D. S. (2016). Two's company, three (or more) is a simplex. *Journal of Computational Neuroscience*, 1–14.
- Giusti, C., Pastalkova, E., Curto, C., & Itskov, V. (2015). Clique topology reveals intrinsic geometric structure in neural correlations. *Proceedings of the National Academy of Sciences of the United States of America*, 112(44), 13455–13460.

- Glahn, D. C., Winkler, A. M., Kochunov, P., Almasy, L., Duggirala, R., Carlsson, M. A., ... Blangero, J. (2010). Genetic control over the resting brain. *Proceedings of the National Academy of Sciences of the United States of America*, 107(3), 1223–1228.
- Glasser, M. F., Coalson, T., Robinson, E., Hacker, C., Harwell, J., Yacoub, E., ... Van Essen, D. C. (2015). A Multi-modal parcellation of human cerebral cortex. *Nature*, 536(7615), 171–178.
- Goodkind, M., Eickhoff, S. B., Oathes, D. J., Jiang, Y., Chang, A., Jones-Hagata, L. B., ... Etkin A. (2015). Identification of a Common Neurobiological Substrate for Mental Illness. *JAMA Psychiatry*, 72(4), 305–315.
- Greicius, M. D., Krasnow, B., Reiss, A. L., & Menon, V. (2003). Functional connectivity in the resting brain: A network analysis of the default mode hypothesis. *Proceedings of the National Academy of Sciences of the United States of America*, 100(1), 253–258.
- Haggard, P., Martin, F., Taylor-Clarke, M., Jeannerod, M., & Franck, N. (2003). Awareness of action in schizophrenia. *Neuroreport*, 14(7), 1081–1085.
- Hassabis, D., Kumaran, D., & Maguire, E. A. (2007). Using imagination to understand the neural basis of episodic memory. *The Journal of Neuroscience: The Official Journal of the Society for Neuroscience*, 27(52), 14365–14374.
- Hastie, T., Tibshirani, R., & Friedman, J. (2001). *The Elements of Statistical Learning*. Heidelberg, Germany: Springer Series in Statistics.
- Hastie, T., Tibshirani, R., & Wainwright, M. (2015). *Statistical Learning with Sparsity: The Lasso and Generalizations*. Boca Raton, FL: CRC Press.
- Holt, D. J., Cassidy, B. S., Andrews-Hanna, J. R., Lee, S. M., Coombs, G., Goff, D. C., ... Moran, J. M. (2011). An anterior-to-posterior shift in midline cortical activity in schizophrenia during self-reflection. *Biological Psychiatry*, 69(5), 415–423.
- Honey, C. J., Sporns, O., Cammoun, L., Gigandet, X., Thiran, J. P., Meuli, R., & Hagmann, P. (2009). Predicting human resting-state functional connectivity from structural connectivity. *Proceedings of the National Academy of Sciences of the United States of America*, 106(6), 2035–2040.
- Horwitz, B., McIntosh, A., Haxby, J., & Grady, C. (1995). Network analysis of brain cognitive function using metabolic and blood flow data. *Behavioural Brain Research*, 66, 187–193.
- Humphreys, G. F., & Ralph, M. A. L. (2015). Fusion and fission of cognitive functions in the human parietal cortex. *Cerebral Cortex (New York, N.Y.: 1991)*, 25(10), 3547–3560.
- Jang, C., Knight, E. Q., Pae, C., Park, B., Yoon, S.-A., & Park, H.-J. (2017). Individuality manifests in the dynamic reconfiguration of large-scale brain networks during movie viewing. *Scientific Reports*, 7, 41414.
- Kanai, R., & Rees, G. (2011). The structural basis of inter-individual differences in human behaviour and cognition. *Nature Reviews Neuroscience*, 12(4), 231–242.
- Kelly, C., Toro, R., Di Martino, A., Cox, C. L., Bellec, P., Castellanos, F. X., & Milham, M. P. (2012). A convergent functional architecture of the insula emerges across imaging modalities. *Neuroimage*, 61(4), 1129–1142.
- Konishi, M., McLaren, D. G., Engen, H., & Smallwood, J. (2015). Shaped by the past: The default mode network supports cognition that is independent of immediate perceptual input. *PLoS One*, 10(6), e0132209.
- Konrad, A., & Winterer, G. (2008). Disturbed structural connectivity in schizophrenia—primary factor in pathology or epiphenomenon? *Schizophrenia Bulletin*, 34(1), 72–92.
- Lee, S. H., DeCandia, T. R., Ripke, S., Yang, J., Sullivan, P. F., Goddard, M. E., ... Wray, N. R. Consortium SPG-WAS. (2012). Estimating the proportion of variation in susceptibility to schizophrenia captured by common SNPs. *Nature Genetics*, 44(3), 247–250.
- Lewis, D. A., & Gonzalez-Burgos, G. (2006). Pathophysiological based treatment interventions in schizophrenia. *Nature Medicine*, 12(9), 1016–1022.
- Liu, Y., Liang, M., Zhou, Y., He, Y., Hao, Y., Song, M., ... Jiang, T. (2008). Disrupted small-world networks in schizophrenia. *Brain: A Journal of Neurology*, 131(4), 945–961.
- Lu, H., Zuo, Y., Gu, H., Waltz, J. A., Zhan, W., Scholl, C. A., ... Stein, E. A. (2007). Synchronized delta oscillations correlate with the resting-state functional MRI signal. *Proceedings of the National Academy of Sciences of the United States of America*, 104(46), 18265–18269.
- Luck, S. J., & Gold, J. M. (2008). The construct of attention in schizophrenia. *Biological Psychiatry*, 64(1), 34–39.
- Lynall, M.-E., Bassett, D. S., Kerwin, R., McKenna, P. J., Kitzbichler, M., Muller, U., & Bullmore, E. (2010). Functional connectivity and brain networks in schizophrenia. *The Journal of Neuroscience: The Official Journal of the Society for Neuroscience*, 30(28), 9477–9487.
- Manoliu, A., Riedl, V., Zherdin, A., Mühlau, M., Schwerthöffer, D., Scherr, M., ... Bäuml, J. (2013). Aberrant dependence of default mode/central executive network interactions on anterior insular salience network activity in schizophrenia. *Schizophrenia Bulletin*, 40(2), 428–437.
- Margulies, D. S., Ghosh, S. S., Goulas, A., Falkiewicz, M., Huntenburg, J. M., Langs, G., ... Petrides, M. (2016). Situating the default-mode network along a principal gradient of macroscale cortical organization. *Proceedings of the National Academy of Sciences of the United States of America*, 113(44), 12574–12579.
- Margulies, D. S., Vincent, J. L., Kelly, C., Lohmann, G., Uddin, L. Q., Biswal, B., ... Petrides, M. (2009). Precuneus shares intrinsic functional architecture in humans and monkeys. *Proceedings of the National Academy of Sciences of the United States of America*, 106(47), 20069–20074.
- Marrelec, G., Krainik, A., Duffau, H., Pelegri-Issac, M., Lehéricy, S., Doyon, J., & Benali, H. (2006). Partial correlation for functional brain interactivity investigation in functional MRI. *Neuroimage*, 32(1), 228–237.
- Mars, R. B., Sallet, J., Schüffelgen, U., Jbabdi, S., Toni, I., & Rushworth, M. F. S. (2012). Connectivity-based subdivisions of the human right “temporoparietal junction area”: Evidence for different areas participating in different cortical networks. *Cerebral Cortex*, 22(8), 1894–1903.
- Maruff, P., Pantelis, C., Danckert, J., Smith, D., & Currie, J. (1996). Deficits in the endogenous redirection of covert visual attention in chronic schizophrenia. *Neuropsychologia*, 34(11), 1079–1084.
- McTeague, L. M., Huemer, J., Carreón, D. M., Jiang, Y., Eickhoff, S. B., & Etkin, A. (2017). Identification of Common Neural Circuit Disruptions in Cognitive Control Across Psychiatric Disorders. *American Journal of Psychiatry*, 174(7), 676–685.
- Meda, S. A., Gill, A., Stevens, M. C., Lorenzoni, R. P., Glahn, D. C., Calhoun, V. D., ... Thaker, G. (2012). Differences in resting-state functional magnetic resonance imaging functional network connectivity between schizophrenia and psychotic bipolar probands and their unaffected first-degree relatives. *Biological Psychiatry*, 71(10), 881–889.
- Medaglia, J. D., Lynall, M.-E., & Bassett, D. S. (2015). Cognitive network neuroscience. *Journal of Cognitive Neuroscience*,
- Menon, V., & Uddin, L. Q. (2010). Saliency, switching, attention and control: A network model of insula function. *Brain Structure and Function*, 214(5–6), 655–667.

- Mesulam, M. M. (1981). A cortical network for directed attention and unilateral neglect. *Annals of Neurology*, 10(4), 309–325.
- Miller, K. L., Alfaro-Almagro, F., Bangerter, N. K., Thomas, D. L., Yacoub, E., Xu, J., ... Smith, S. M. (2016). Multimodal population brain imaging in the UK Biobank prospective epidemiological study. *Nature Neuroscience*, 19(11):1523–1536.
- Northoff, G., & Qin, P. (2011). How can the brain's resting state activity generate hallucinations? A 'resting state hypothesis' of auditory verbal hallucinations. *Schizophrenia Research*, 127(1), 202–214.
- Öngür, D., Lundy, M., Greenhouse, I., Shinn, A. K., Menon, V., Cohen, B. M., & Renshaw, P. F. (2010). Default mode network abnormalities in bipolar disorder and schizophrenia. *Psychiatry Research*, 183(1), 59–68.
- Pankow, A., Deserno, L., Walter, M., Fydrich, T., Bermpohl, F., Schlagenhauft, F., & Heinz, A. (2015). Reduced default mode network connectivity in schizophrenia patients. *Schizophrenia Research*, 165(1), 90–93.
- Potkin, S., Turner, J., Brown, G., McCarthy, G., Greve, D., Glover, G., ... Wible, C. (2009). Working memory and DLPFC inefficiency in schizophrenia: the FBBIRN study. *Schizophrenia Bulletin*, 35(1), 19–31.
- Raichle, M. E. (2015). The brain's default mode network. *Annual Review of Neuroscience*, 38, 433–447.
- Raichle, M. E., MacLeod, A. M., Snyder, A. Z., Powers, W. J., Gusnard, D. A., & Shulman, G. L. (2001). A default mode of brain function. *Proceedings of the National Academy of Sciences of the United States of America*, 98(2), 676–682.
- Ripke, S., Neale, B. M., Corvin, A., Walters, J. T., Farh, K.-H., Holmans, P. A., ... O'Donovan, M. C. (2014). Biological insights from 108 schizophrenia-associated genetic loci. *Nature*, 511(7510), 421–427.
- Rosenberg, M. D., Finn, E. S., Scheinost, D., Papademetris, X., Shen, X., Constable, R. T., & Chun, M. M. (2015). A neuromarker of sustained attention from whole-brain functional connectivity. *Nature Neuroscience*, 19(1), 165–171.
- Rotarska-Jagiela, A., van de Ven, V., Oertel-Knöchel, V., Uhlhaas, P. J., Vogelzey, K., & Linden, D. E. (2010). Resting-state functional network correlates of psychotic symptoms in schizophrenia. *Schizophrenia Research*, 117(1), 21–30.
- Rottschy, C., Langner, R., Dogan, I., Reetz, K., Laird, A. R., Schulz, J. B., ... Eickhoff, S. B. (2012). Modelling neural correlates of working memory: a coordinate-based meta-analysis. *Neuroimage*, 60(1), 830–846.
- Salomon, J. A., Vos, T., Hogan, D. R., Gagnon, M., Naghavi, M., Mokdad, A., ... Jonas, J. B. (2013). Common values in assessing health outcomes from disease and injury: disability weights measurement study for the Global Burden of Disease Study 2010. *The Lancet*, 380(9859), 2129–2143.
- Sato, Y., Yabe, H., Todd, J., Michie, P., Shinozaki, N., Sutoh, T., ... Kaneko, S. (2003). Impairment in activation of a frontal attention-switch mechanism in schizophrenic patients. *Biological Psychology*, 62(1), 49–63.
- Satterthwaite, T. D., Elliott, M. A., Gerraty, R. T., Ruparel, K., Loughead, J., Calkins, M. E., ... Wolf, D. H. (2013). An improved framework for confound regression and filtering for control of motion artifact in the preprocessing of resting-state functional connectivity data. *Neuroimage*, 64, 240–256.
- Schurz, M., Radua, J., Aichhorn, M., Richlan, F., & Perner, J. (2014). Fractionating theory of mind: A meta-analysis of functional brain imaging studies. *Neuroscience and Biobehavioral Reviews*, 42, 9–34.
- Seeley, W. W., Menon, V., Schatzberg, A. F., Keller, J., Glover, G. H., Kenna, H., ... Greicius, M. D. (2007). Dissociable intrinsic connectivity networks for salience processing and executive control. *The Journal of Neuroscience: The Official Journal of the Society for Neuroscience*, 27(9), 2349–2356.
- Seghier, M. L. (2013). The Angular Gyrus: Multiple Functions and Multiple Subdivisions. *The Neuroscientist*, 43–61.
- Shalev-Shwartz, S., & Ben-David, S. (2014). *Understanding machine learning: From theory to algorithms*: Cambridge University Press.
- Shim, G., Oh, J. S., Jung, W. H., Jang, J. H., Choi, C.-H., Kim, E., ... Kwon, J. S. (2010). Altered resting-state connectivity in subjects at ultra-high risk for psychosis: an fMRI study. *Behavioral and Brain Functions*, 6(1), 58.
- Smith, S. M., Nichols, T. E., Vidaurre, D., Winkler, A. M., Behrens, T. E. J., Glaser, M. F., ... Miller, K. L. (2015). A positive-negative mode of population covariation links brain connectivity, demographics and behavior. *Nature Neuroscience*, 18(11), 1565–1567.
- Spreng, R. N., Mar, R. A., & Kim, A. S. N. (2009). The common neural basis of autobiographical memory, prospection, navigation, theory of mind, and the default mode: A quantitative meta-analysis. *Journal of Cognitive Neuroscience*, 21(3), 489–510.
- Stephan, K. E., Binder, E. B., Breakpear, M., Dayan, P., Johnstone, E. C., Meyer-Lindenberg, A., ... Fletcher, P. C. (2016). Charting the landscape of priority problems in psychiatry, part 2: Pathogenesis and aetiology. *The Lancet. Psychiatry*, 3(1), 84–90.
- Stephan, K. E., Friston, K. J., & Frith, C. D. (2009a). Dysconnection in Schizophrenia: From Abnormal Synaptic Plasticity to Failures of Self-monitoring. *Schizophrenia Bulletin*, 35(3), 509–527.
- Stephan, K. M., Fink, G. R., Passingham, R. E., Silbersweig, D., Ceballos-Baumann, A. O., Frith, C. D., & Frackowiak, R. S. (1995). Functional anatomy of the mental representation of upper extremity movements in healthy subjects. *Journal of Neurophysiology*, 73(1), 373–386.
- Tibshirani, R. (1996). Regression shrinkage and selection via the lasso. *Journal of the Royal Statistical Society. Series B (Methodological)*, 267–288.
- van den Heuvel, M. P., Mandl, R. C., Stam, C. J., Kahn, R. S., & Pol, H. E. H. (2010). Aberrant frontal and temporal complex network structure in schizophrenia: a graph theoretical analysis. *Journal of Neuroscience*, 30(47), 15915–15926.
- Varoquaux, G., Gramfort, A., Poline, J.-B., & Thirion, B. (2010). Brain covariance selection: better individual functional connectivity models using population prior. *Advances in Neural Information Processing Systems*, 23:234–242.
- Vogt, B. A., & Laureys, S. (2005). Posterior cingulate, precuneal and retrosplenial cortices: cytology and components of the neural network correlates of consciousness. *Progress in Brain Research*, 150, 205–217.
- Vogt, B. A., & Pandya, D. N. (1987). Cingulate cortex of the rhesus monkey: II. Cortical afferents. *The Journal of Comparative Neurology*, 262(2), 271–289.
- Wang, H.-T., Giulia, P., Charlotte, M., Bzdok, D., Jefferies, E., & Smallwood, J. (2017). Dimensions of Experience: Exploring the Heterogeneity of the Wandering Mind. *Psychological Science*.
- Weinberger, D. R., Berman, K. F., Suddath, R., & Torrey, E. F. (1992). Evidence of dysfunction of a prefrontal-limbic network in schizophrenia: A magnetic resonance imaging and regional cerebral blood flow study of discordant monozygotic twins. *The American Journal of Psychiatry*, 149(7), 890–897.
- Westlye, L. T., Grydeland, H., Walhovd, K. B., & Fjell, A. M. (2011). Associations between regional cortical thickness and attentional networks as measured by the attention network test. *Cerebral Cortex (New York, N.Y.: 1991)*, 21(2), 345–356.

- White, T. P., Joseph, V., Francis, S. T., & Liddle, P. F. (2010). Aberrant salience network (bilateral insula and anterior cingulate cortex) connectivity during information processing in schizophrenia. *Schizophrenia Research*, 123(2), 105–115.
- Whitfield-Gabrieli, S., & Ford, J. M. (2012). Default mode network activity and connectivity in psychopathology. *Annual Review of Clinical Psychology*, 8, 49–76.
- Whitfield-Gabrieli, S., Thermenos, H. W., Milanovic, S., Tsuang, M. T., Faraone, S. V., McCarley, R. W., ... Seidman, L. J. (2009). Hyperactivity and hyper-connectivity of the default network in schizophrenia and in first-degree relatives of persons with schizophrenia. *Proceedings of the National Academy of Sciences of the United States of America*, 106(4), 1279–1284.
- Woodward, N. D., Rogers, B., & Heckers, S. (2011). Functional resting-state networks are differentially affected in schizophrenia. *Schizophrenia Research*, 130(1), 86–93.
- Yu, Q., Sui, J., Kiehl, K. A., Pearlson, G., & Calhoun, V. D. (2013). State-related functional integration and functional segregation brain networks in schizophrenia. *Schizophrenia Research*, 150(2), 450–458.
- Zhou, Y., Liang, M., Tian, L., Wang, K., Hao, Y., Liu, H., ... Jiang, T. (2007). Functional disintegration in paranoid schizophrenia using resting-state fMRI. *Schizophrenia Research*, 97(1), 194–205.

SUPPORTING INFORMATION

Additional Supporting Information may be found online in the supporting information tab for this article.

How to cite this article: Lefort-Besnard J, Bassett DS, Smallwood J, et al. Different shades of default mode disturbance in schizophrenia: Subnodal covariance estimation in structure and function. *Hum Brain Mapp*. 2018;39:644–661. <https://doi.org/10.1002/hbm.23870>

SUPPORTING INFORMATION APPENDIX

"Different shades of default mode disturbance in schizophrenia:
Subnodal covariance estimation in structure and function."

Jérémie Lefort-Besnard, Danielle S. Bassett, Jonathan Smallwood, Daniel Margulies, Birgit Derntl, Oliver Gruber, Andre Aleman, Renaud Jardri,
Gaël Varoquaux, Bertrand Thirion, Simon B. Eickhoff and Danilo Bzdok

Contents:

1. Supplementary Tables (3)
2. Supplementary Figures (1)

1. Supplementary tables

Supplementary Table 1: Demographic information on participants

Site	Group	Age	Age Difference (p value)	Female	Male	n	N
Groningen	HC	31.6		13	19	32	
Groningen	SZ	33.6	0.476	13	19	32	64
Göttingen	HC	31.9		7	22	29	
Göttingen	SZ	32.0	0.978	6	27	33	62
Aachen	HC	33.2		3	10	13	
Aachen	SZ	35.1	0.682	3	11	14	27
Lille	HC	29.0		5	11	16	
Lille	SZ	33.3	0.048	6	9	15	31
COBRE	HC	35.8		23	50	73	
COBRE	SZ	38.2	0.270	13	55	68	141
Σ	HC	33.4		51	112	163	
	SZ	35.3	0.491	41	121	162	325

Supplementary Table 2: Information on MRI scanning sites

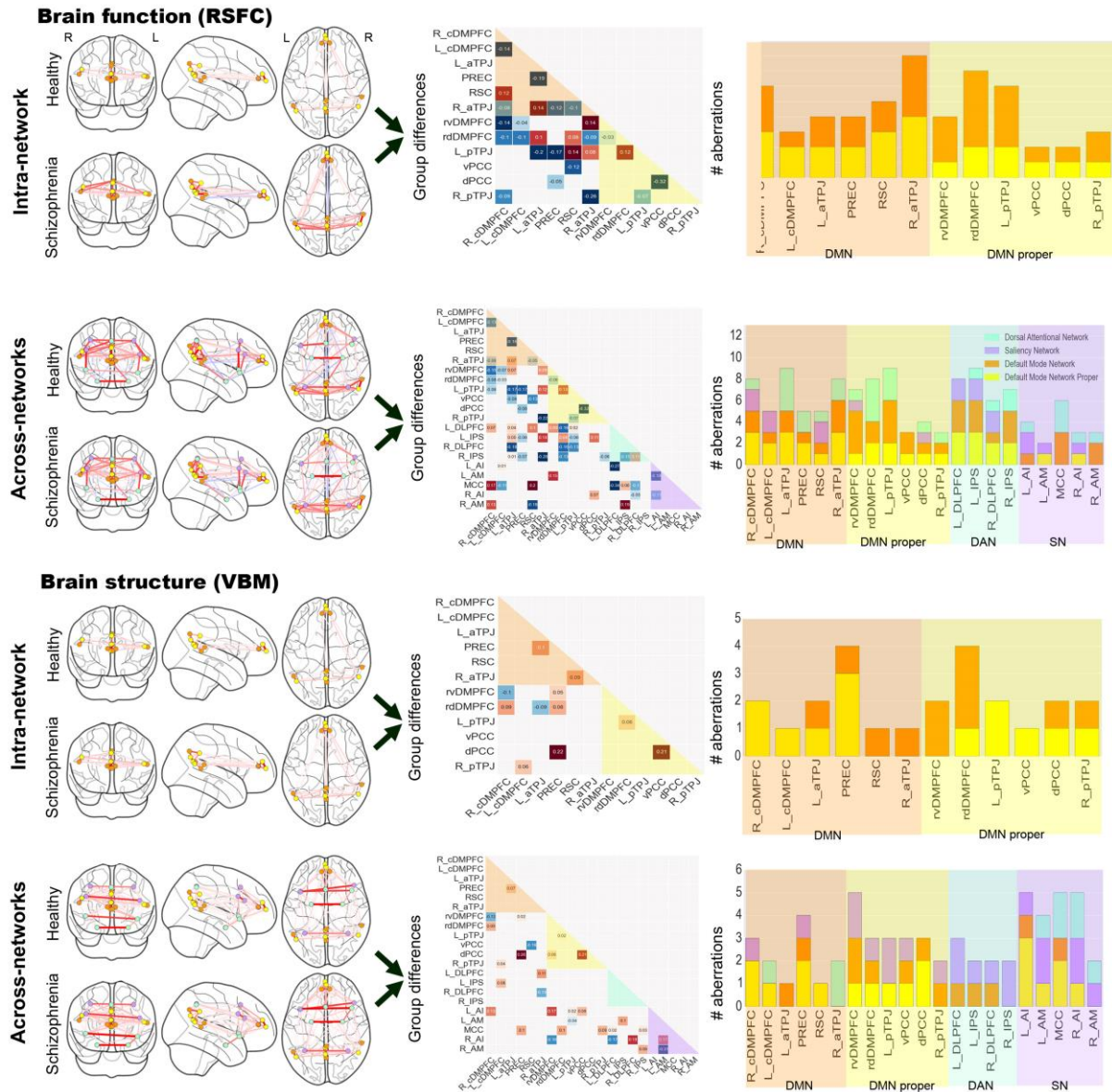
Place	Aachen	Gröningen	Göttingen	Lille	COBRE
Scanner	Siemens 3T TrioTim	Philips Achieva 3 T	Siemens TrioTim	Philips Achieva 3T	Siemens 3T TrioTim
TR (ms)	2000	2400	2000	1000	2000
TE (ms)	28	28	30	9,6	29
Number of slices	34	43	33	45	32
Slice- thickness (mm)	3,3	3	3	3,4	3,5
Gap (mm)	3,6	n.a	0,6	n.a	1
Flip-angle	77	85	70	9	
Voxel-size (mm3)	n.a	n.a	n.a	3,219 x 3,219 x 3,4 mm	3 x 3 x 4mm3
Orientation	Axial	Axial	Axial	Sagittal	Axial
In-plane resolution (mm2)	3,6 x 3,6	3,44 x 3,44	3 x 3	n.a	3,75 x 3,75
Cross hair	Yes	No, eyes closed	Yes	No, eyes closed	Yes

Supplementary Table 3: coordinate per ROIs

	seeds definition	Full name	x	y	z	number voxel
DMN nodes	DMPFC	Dorsomedial prefrontal cortex	0	55,86	14,6	318
	PMC	Posterior Medial cortex	-0,3	-53,67	29,3	1518
	R_TPJ	Right temporo-parietal junction	55,56	-47,31	16,73	239
	L_TPJ	Left temporo-parietal junction	-49,66	-57,94	24,9	376
DMN subnodes	R_cDMPFC	Caudal right dorsomedial prefrontal cortex	6,82	49,02	13,43	44
	rvDMPFC	Rostro-ventral dorsomedial prefrontal cortex	-0,6	61,05	9,84	100
	rdDMPFC	Rostro-dorsal dorsomedial prefrontal cortex	0,97	55,46	21,08	74
	L_cDMPFC	caudal left dorsomedial prefrontal cortex	-6,36	48,57	13,78	42
	PREC	Precuneus	1,08	-63,02	37,97	357
	vPCC	Ventral posterior cingulate cortex	-0,35	-57,15	20,97	291
	dpCC	Dorsal posterior cingulate cortex	0,057	-46,48	34,76	420
	RSC	Retrosplenial cortex	1,26	-44,26	9,96	82
	R_aTPJ	Anterior right temporo-parietal junction	58,62	-38,85	16,16	98
	R_pTPJ	Posterior right temporo-parietal junction	53,32	-54,5	17,47	119
DAN	L_aTPJ	Anterior left temporo-parietal junction	-52,14	-53,32	20,48	163
	L_pTPJ	Posterior left temporo-parietal junction	-47,76	-61,48	28,28	213
	L_DLPFC	Left dorsolateral prefrontal cortex	-40,75	15,96	31,22	966
	R_DLPFC	Right dorsolateral prefrontal cortex	46,25	26,46	24,26	505
SN	R_IPS	Right intraparietal sulcus	36,39	-51,63	46,05	373
	L_IPS	Left intraparietal sulcus	-33,78	-51,44	47,49	565
	R_AM	Right amygdala	27,59	-4,1	-19,73	172
	L_AM	Left amygdala	-23,04	-4,46	-19,64	157
	R_AI	Right anterior insula	42,57	18,03	-5,8	309
	L_AI	Left anterior insula	-41,42	16,8	-0,84	218
	MCC	Mid cingulate cortex	0,11	19,69	46	338

2. Supplementary Figures

Supplementary figure 1:



DMN aberrations in schizophrenia are specific to subnodes.

Functional connectivity (RSFC) and structural co-occurrence (VBM) measurements were used to compute sparse inverse covariance estimation separately in healthy and schizophrenic individuals (*left column*). We conducted intra-network analyses (i.e., DMN subnode atlas) and across-network analyses (i.e., DMN subnode atlas augmented by nodes of the DAN and SN). Statistically significant group differences (*squares* in the *middle column*) with direction and intensity of the differences (*shades of blue* for hyper-coupling, *shades of red* for hypo-coupling) between the normal and diagnosed individuals are shown in the precision

matrix of the schizophrenia group. The number of subnode-specific dysregulations is shown as counts when viewed from the DMN proper (*yellow*), other DMN parts (*orange*), DAN (*light green*), and SN (*purple*). The findings make apparent that schizophrenia pathophysiology may be relatively more driven by across-network effects and effects outside of the DMN proper. The glass brains were created using the nilearn Python package (Abraham et al., 2014).

SUPPORTING INFORMATION APPENDIX

"Patterns of Schizophrenia Symptoms: Hidden Structure in the PANSS Questionnaire"

Jérémie Lefort-Besnard, Gaël Varoquaux, Birgit Derntl, Oliver Gruber, Andre Aleman,
Renaud Jardri, Iris Sommer, Bertrand Thirion, Danilo Bzdok

Contents:

1. Supplementary methods (4 pages)
2. Supplementary results (1 page)
3. Supplementary discussion (1 pages)
4. Supplementary figures (3 pages)
5. Supplementary table (1 page)
6. Bibliography (1 page)

1. SUPPLEMENTARY METHODS

Data resources

We revisited the underlying structure of the PANSS questionnaire based on behavioral data from eight different schizophrenia samples acquired in Europe and the USA: Goettingen, Groeningen, Lille, Utrecht, Tuebingen, COBRE, as well as two different samples from Aachen (see Supplementary Table 1 for details). The behavioral assessments were collected from a total of 218 patients, including 154 males and 64 female subjects. Three patients were excluded from the study due to missing items scores in the PANSS questionnaire. The mean age across the eligible participants was 35.3 years (S.D. = 11.42; ranging from 18 to 65), which did not yield a statistically significant difference between males and females ($p=0.26$). Each subject has been diagnosed by a board-certified psychiatrist in accordance with the clinical criteria of the International Classification of Diseases (ICD-10) or the Diagnostic and Statistical Manual of Mental Disorders (DSM-IV-TR). All patients underwent a 40-45min semi-structured clinical interview with a medical doctor, after which the clinician rated the patient on the 30 PANSS items. The distribution of the PANSS questionnaire responses in our sample was homogeneous (Fig. 1). Ethics approvals were obtained from the ethics committee of each site's university.

Identifying the hidden item stratification: Principal component analysis

PCA is the most commonly applied data-analysis method that was previously used to discover hidden factors of variation in the PANSS questionnaire. We therefore applied the same statistical approach to our sample of schizophrenia patients as a point of comparison to previous research.

PCA summarizes the PANSS items scores into a smaller number of representative variables that collectively explain most of the variability across the set of original questionnaire items. The idea is that not all of the 30 PANSS items are equally effective in describing schizophrenia symptoms. PCA seeks weighted combinations of the items that are as interesting as possible, where the concept of *interesting* is measured by the amount that patient scores vary along each emerging dimension. More concretely, PCA explored the relationships between the 30 questionnaire items and exhibits them as a

linear combination of uncorrelated variables called *principal components*. Each such component of symptom variation is represented as a set of specific weights for the questionnaire items, one item weight for each hidden variability component. All weights of a given component are typically non-zero in contrast to the sparse modeling approach below. The weights of the first principal component define the most important source of variation that is as close as possible to the patient symptom scores as its direction is indicative of how response profiles vary the most. In other words, the first principal component i) captures a maximum of the information contained in the set of PANSS items, ii) identifies a direction along which the patient scores vary the most, and iii) provides the linear fit that is closest to the patients' clinical profile. The second principal component, in turn, is a linear combination of the PANSS items that is uncorrelated with the first principal component and extracts the largest direction of variance under this constraint. The strategy is analogous for the third and all subsequent extracted components. Each additional principal component must ensure uncorrelatedness to the previous ones while explaining the largest portion of unexplained variance.

The majority of previous studies revisiting the PANSS reported five-component solutions. We hence compared the similarities between the five PCA directions extracted from our patient sample and the five latent components found in other psychiatric populations (1-3).

Identifying hidden group structure: k-means clustering

We applied a k-means clustering algorithm to automatically partition patient symptom profiles into homogeneous groups. PCA and k-mean pursued complementary statistical goals in our study, although both these structure-discovery methods simplify the response items into a smaller number of summary scores. While PCA extracts representations of the data explaining most of the variance, k-means finds homogeneous groups among the observed symptom profiles from the patients. Here, the goal was to partition patients into discrete groups so that patients within each group are quite similar to each other in terms of their salient symptoms, while patients in different groups are maximally different from each other. In other words, this common clustering technique automatically establishes k groups that are internally coherent in their presented symptoms but as different as possible from each other. In contrast to PCA, k-means is a method identifying one-to-many mappings (4): each patient is a member of exactly one group. k-means seeks to partition patient symptom profiles into a number of non-overlapping patient groups. k-means requires to prespecify the desired number of groups k . We thus used "NbClust" (5), an established R package that simultaneously applied 30 cluster validity metrics. This approach provided complementary indications of the number of groups most supported by the patient data. Among all indices (using the method "median") and according to the majority rule, the best number of clusters was 3. That is, the most robust three groups were expressed in the final clustering solution. Therefore, three patient groups of distinct symptom profiles were automatically extracted as it provided a useful fit to our clinical sample.

Identifying predictive structure: Sparse logistic regression

The goal of PCA and k-means was to discover interesting symptoms patterns as measured by PANSS items such as underlying structure and relationship among schizophrenia patients. Complementing these insights in a next step, we applied a modeling technique that emphasizes both prediction performance and automatic identification of the most relevant items. That is, we wanted to fit a model that i) relates

the item scores to the severity of schizophrenia, with the aim of accurately predicting the response for future patient (i.e., out-of-sample prediction) and ii) finds the most parsimonious subsets of predictive PANSS items.

To achieve this goal, we capitalized on the pattern-learning algorithm *sparse logistic regression* (6). On the one hand, this predictive learning algorithm estimates the separating hyperplane (i.e., a linear function) that distinguishes patients with more severe versus more mild schizophrenia symptoms. The outcome y is defined by the severity of schizophrenia. The severity is characterized by the median-split of the PANSS total score (0 as mild, 1 as severe) as it was the categorical summary of the constituent continuous scores. On the other hand, the imposed sparsity constraint identifies a minimal subset of features (i.e., items of the PANSS questionnaire) that is most informative about the differences between patients. While computing a vector of weights associated with the items, similar to linear regression, this approach aims to reduce the weights of items that have little discriminatory value to exactly zero (a feature's weight equal to zero has no effect on the prediction outcome). This procedure results in a subselection of items which have high joint discriminatory power to separate patients with severe versus mild symptoms. In this way, sparse logistic regression extends previous PANSS investigations by automatic *variable selection* (7). Its benefit is rooted in its clear algorithmic definition leading to formal and rigorous choices in automatic variable selection. This additional constraint enforcing parsimony of response items is particularly useful in our study, as it helps pointing to subset of items most predictive of schizophrenia severity. As a result, our modeling findings obtained from the sparse logistic regression are much easier to interpret.

The sparsity constraint was imposed in form of an ℓ_1 regularization. Such a constraint in the optimization objective automatically detects relevant features “on-the-fly” during model estimation. The ℓ_1 penalty term, calibrated by the hyper-parameter λ , is designed to control the parsimony criterion and its shrinkage regularization on the learned model weights. This penalized (negative) log likelihood of the logistic regression objective is given by:

$$-\frac{1}{N} \sum_{i=1}^N \log(1 + e^{-y_i f(x_i; \beta_0, \beta)}) + \lambda \|\beta\|_1$$

where x_i represents a given patient's PANSS scores, y_i is his/her schizophrenia severity, β_0 is the intercept, and β is the weight attached to each questionnaire item, the right part of the equation corresponds to the ℓ_1 penalty term controlled by the hyper-parameter λ . The item selection behavior depends on the choice of this tuning parameter. Indeed, the sparse logistic regression shrinks the coefficient estimates more toward zero and performs always more aggressive variable selection with increasing λ . The hyper-parameter selection was based on the data in a principled fashion using nested cross-validation. In a common grid of candidate parameter choices, the value of λ was varied logarithmically from 3.5 to 1.0 in log-space with 16 steps. The member in the model family that yielded highest prediction accuracy (i.e., generalization performance) for each candidate of λ was selected. In this way, the quantitative investigation detected subsets of items that were most predictive for schizophrenia severity. In other words, the goal here was not to select the best hyperparameter. Rather, we charted a space of candidate λ to explicitly investigate the transition from low to high sparsity.

Finally, we further detailed this analysis with an examination of the learning curve to assess the predictive model performance as a function of increasing sample size. To this

end, we computed the prediction accuracy for the sparse logistic regression for predicting schizophrenia severity in a series of increasing patient subsets for model training.

Testing for complex relationships among the PANSS items

The k-means method (cf. above) extracted latent structure dormant in the data regardless of symptom severity measures. Sparse logistic regression (cf. above) in turn selected the most predictive variables but this predictive algorithm was not convenient to uncover hidden non-linear relationships between the questionnaire items. We combined exploration of more sophisticated item-item relationships with evaluating prediction performance using non-linear predictive algorithms. In this way, we tested the hypothesis of existing higher-order relationships between the PANSS responses and their usefulness for prediction. We compared the performance of linear models to the performance of models able to exploit non-linear structure in the questionnaires. We complemented this analysis with accuracy-sample-size examination by computing learning curve for each pattern-learning model. Three linear models (ridge regression, logistic regression, and support vector machine) were benchmarked against three models allowing looking for higher-order interactions (k nearest neighbor, random forest and adaptive boosting). Again, schizophrenia severity was defined as the median-split of the PANSS total score (0 as mild, 1 as severe) representing a categorical summary of the constituent continuous scores.

Among the linear predictive pattern-learning algorithms, the ridge regression is commonly used as a shrinkage method. This model encourages small absolute weights on each item which emphasized the most predictive PANSS items, while linear support vector machines mapped the items as points in space so that items of separate categories (predictive of a mild or a severe schizophrenia) were divided by a maximal gap between the patients.

Regarding the non-linear models, the k nearest neighbor estimator uses the k closest training examples (in our case, the closest patient symptom profiles) in the feature space, while the output is determined by a majority vote across these most similar training examples. In other words, the guessed severity for a given new schizophrenia patient can thus be derived from the schizophrenia severity of the k closest patients in the training set. Further, the random forest algorithm is an ensemble learning method that operates by constructing a multitude of decision trees and outputs its prediction estimate that is the committee decision across all trees. The severity of schizophrenia symptoms in a given patient was thus derived based on the most consistently predicted outcome of the built decision trees. As the last non-linear prediction algorithm, the adaptive boosting algorithm starts by fitting a model on the dataset and then fits additional copies of that model on the same dataset but where the weights of incorrectly judged instances are adjusted such that subsequent fine-tuning of models focusses more on difficult cases.

Code availability

Python was selected as scientific computing engine. Capitalizing on its open-source ecosystem helps enhance replicability, reusability, and provenance tracking. Scikit-learn (8) provided efficient, unit-tested implementations of state-of-the-art statistical learning algorithms (<http://scikit-learn.org>). All analysis scripts of the present study are readily accessible to the reader online (<https://github.com/JLefortBesnard/Panss2018>).

2. SUPPLEMENTARY RESULTS

Comparison to previous hidden-factor investigations

In a preparatory analysis, we replicated the most often used statistical approach for latent-factor modeling of the PANSS questionnaire administered to schizophrenia patients (SFig. 1). We computed the five dominant components of variation in our multi-site sample using PCA analogous to previous studies (1-3). Our findings from the five-component solution were found to be virtually identical to the previously reported findings in other schizophrenia populations (1-3).

The present PCA decomposition of PANSS items explained 52% of the variance across symptom scales. This result in our sample is similar to what was found in previous studies: 52% (2), 51% (3), up to 57% of variance explained (1). The component most associated with negative symptom items captured the largest amount of the total variance (26%). Several PANSS items were found to be important in both the first component extracted from our dataset and in the first component derived from other patient samples (1-3). This first component was mostly associated with negative symptom items, including disturbance of volition, passive/apathetic social withdrawal, active social avoidance, motor retardation, and emotional withdrawal from the highest to the lowest absolute association. Our second component exhibited most associations with various positive symptom items (10% explained variance). Three items with relevant weights were found both in our component as well as in the component associated with positive symptom items discovered in previous studies (1-3). These items included grandiosity, unusual thought content, and delusions (from highest to lowest weight relevance). The three remaining components explained approximately 5% of the variance each. A component associated with excitement symptoms had two highly weighted items in common with the excitement-related component of previous studies including from the highest to the lowest absolute association poor impulse control and uncooperativeness (1-3). The five items preoccupation, mannerisms and posturing, stereotyped thinking, conceptual disorganization, lack of judgement and insight (ordered from the highest to the lowest absolute weight) were found relevant in our fourth component as well as in previously reported components mostly associated with cognitive symptom (1-3). Finally, the fifth component exposed three relevant items that were also highlighted in the component related to emotional discomfort symptom in previous studies (1-3), including tension, somatic concern, and preoccupation (from the highest to the lowest absolute weight).

In sum, carrying out PCA on PANSS questionnaires from a large schizophrenia sample led to virtually identical directions of variation patterns underlying symptom combinations as in previous factor modeling investigations. Furthermore, the discovered variability components that explained most of the variance prominently included PANSS items associated with negative symptom. Instead, PANSS items from the positive and general scales were more inconsistently emphasized across the components of variation, which is in line with previous findings (1-3).

3. SUPPLEMENTARY DISCUSSION

Extracting continuous axes in the PANSS

Our investigation set out by replicating the often reported latent-factor results obtained from the principal components of the PANSS questionnaire administered to schizophrenia patients. To evaluate correspondence with a stream of previous PANSS studies, we extracted five most dominant components in our sample. In agreement with previous research, these five directions of variation indicated that symptomatology varies along negative, positive, excitement, cognitive and emotional discomfort symptoms items from the highest to the lowest influence.

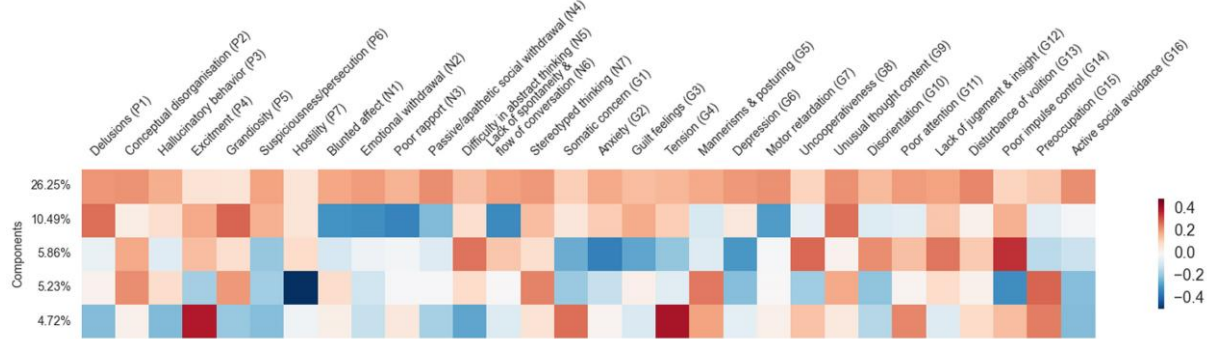
Over more than 30 years, insightful information about schizophrenia psychopathology was obtained through the extraction of hidden dimensions in the PANSS questionnaire using an essentially identical statistical tool: principal component analysis. Most studies of clinical behavior have probed item patterns of five overarching components underlying the PANSS questionnaire. An overwhelming majority of previous studies reported a component with relevant loadings on negative symptom items as explaining most of the variance (1-3). Here, we replicated this recurring finding across over a dozen of previous PANSS questionnaire investigations. Indeed, most of the response variability was explained by the component with relevant loadings on negative symptoms items. This first component can be viewed as the direction along which the patient scores are highly variable. Another recurring finding includes a component with relevant loadings on positive symptom items which was also replicated in our sample (1-3). The three other components were also similar to the previous findings as their loadings emphasized variation over an excitement, cognitive, and emotional discomfort syndrome. In this set of preparatory analyses, our results confirmed virtually identical symptom gradients underlying PANSS questionnaire scores suggesting similarities in the underlying properties present in our multi-site dataset and those present in samples from other PANSS investigations.

Analogous to previous studies (1-3), our sample analysis revealed no item associated with positive symptoms that has high loadings in the first component associated with negative symptoms. This observation corroborates previous findings supporting the notion that the negative symptoms represent a source of variation separate from other symptom aspects in schizophrenia. Indeed, across studies, negative symptoms consistently emerged as a separate factor (9). Instead, across previous PCA analyses, PANSS items from the positive and general scales were more inconsistently associated with components of variation (1-3). Explanations for the observed divergences may include that different subgroups of schizophrenia patients differ less systematically in their symptom patterns that are different from the negative symptoms.

In sum, our results are in line with the pentagonal model of representation of PANSS, which defines five hidden factors summarizing schizophrenia patients PANSS scores (3). The pentagonal model includes variation over negative, positive, activation, dysphoric mood and autistic preoccupation symptoms items which mostly corroborate other findings (1, 2) including ours. We indeed obtained five virtually identical directions of variation patterns underlying PANSS questionnaire scores. In other words, we have shown that our sample harbors very similar emerging properties than most of the previously explored schizophrenia patients samples.

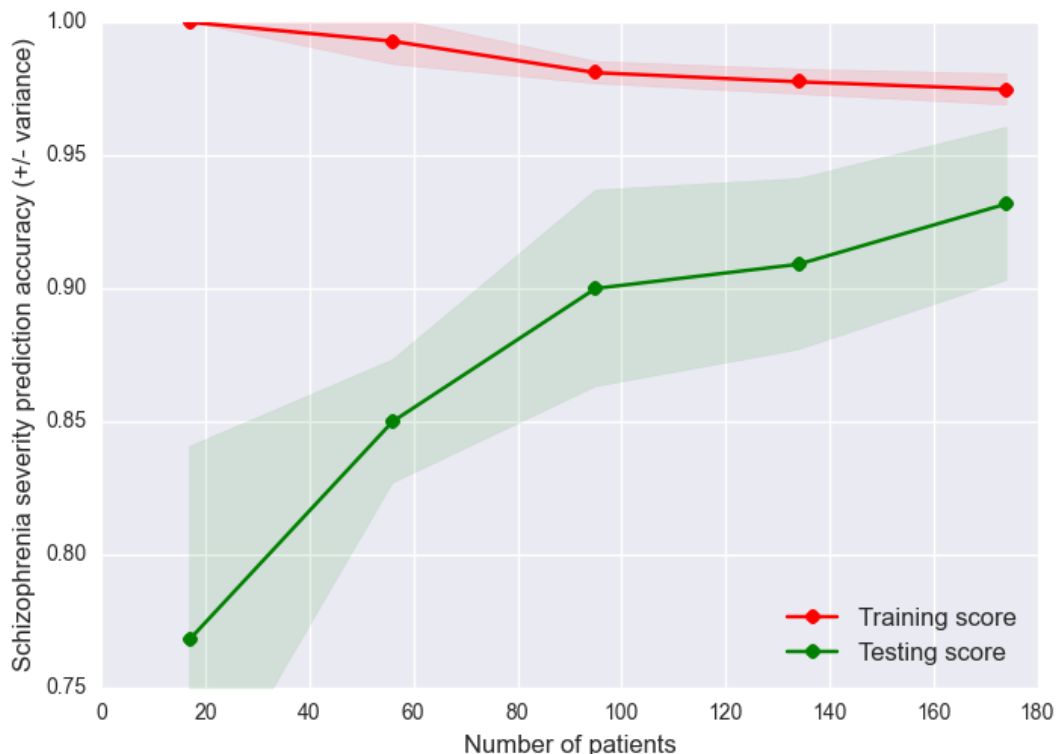
4. SUPPLEMENTARY FIGURES

Supplementary figure 1



Replication of the previous PCA approaches to decomposing PANSS questionnaire. We carry out commonly used principal component analysis to derive five components of variation in the PANSS questionnaire data in our patient sample. Each component and its ratio of explained variance are shown. Each row shows the item relevance (weights) for each component. The findings confirmed earlier descriptions of five components, each closely and specifically associated with a particular schizophrenia symptom including negative, positive, excitement, cognitive and emotional discomfort symptoms. Among these, we obtained one component roughly corresponding to each group of symptoms. Our five-component solution was virtually identical to the components found in a series of previous hidden factor decompositions in schizophrenic patient samples (1-3).

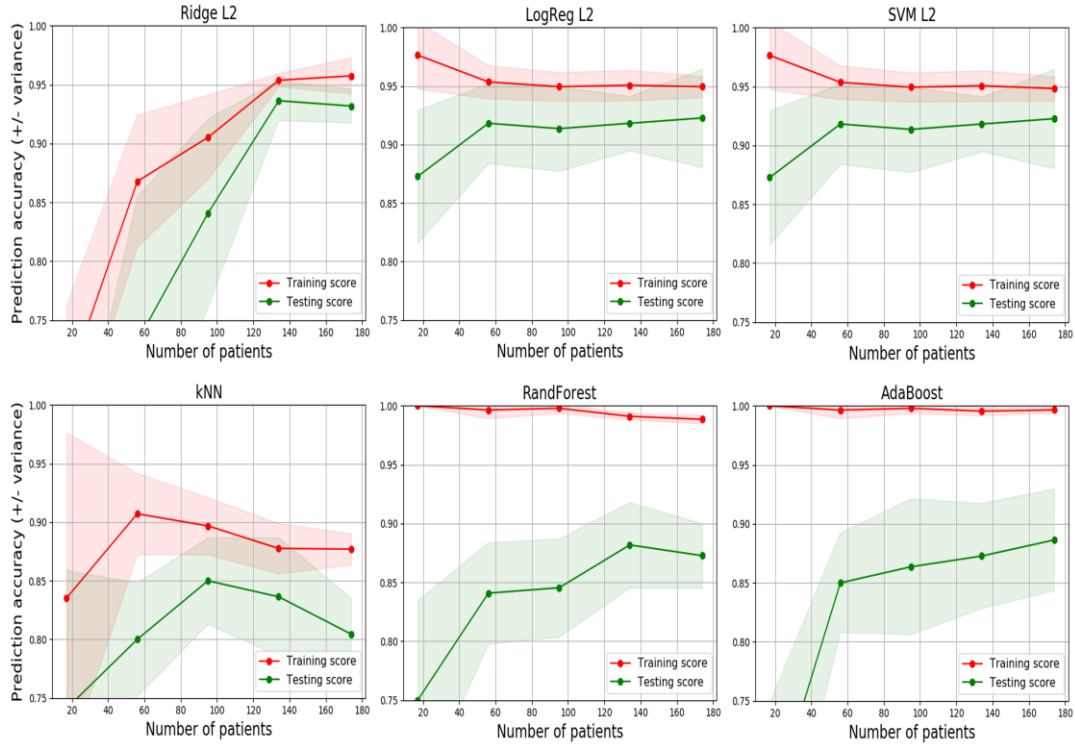
Supplementary figure 2



Scaling of schizophrenia prediction accuracy with increasing patients.

A learning curve is a representation of performance of the learning algorithm with always bigger subsets of the data at hand. The number of patients included is plotted on the x axis while the y axis displays the obtained accuracy for each specific setting (5 splits of the total amount of available data). The *red line* represents the average in-sample (i.e., *training score*) accuracy, while the green line represents the average generalization performance (i.e., *testing score*). The green and red shadows represent the accuracy standard deviations. Performance in the training set higher than performance in the testing set is to be expected since the training score can dramatically overestimate the test score. Indeed, the learning algorithm learns from the training data and therefore is optimistically biased while the test score represents the efficiency of the model applied to unseen data. While recruitment of more patients would likely further improve the performance of the learning algorithms, we can observe that gathering 90 subjects is a good tradeoff between the needed amount of data and achieving a fair classifier performance.

Supplementary figure 3



Scaling of linear and non-linear prediction accuracy with increasing patients.

We explored the learning behavior of each model with always bigger subsets of the data at hand, in the same fashion as the analysis in supplementary figure 2. The learning curve of each linear model (Ridge Regression, Logistic Regression and SVM) is plotted on the first row while the learning curve of each non-linear model (kNN, Random Forest, and Adaptive Boosting) is plotted on the second row. The number of patients whose data is considered is given on the x axis, while the y axis displays the obtained accuracy for each specific setting (5 splits of the total amount of available data). The *red line* represents the average in-sample (i.e., *training score*) accuracy, while the green line represents the average expected generalization performance (i.e., *testing score*). The green and red shadows represent the accuracy standard deviation. We can observe that gathering around 130 subjects is a good tradeoff between the needed amount of data and achieving a fair classifier performance for both the linear and non-linear models. On the other hand, recruitment of more patients may likely further improve the performance in more data-hungry non-linear models, such as the AdaBoost.

5. SUPPLEMENTARY TABLE

Supplementary table 1:

Sites	# patients	# male	# female	Age (M)	Age (Std)	Age onset (M)	Age onset (Std)
Aachen	28	20	8	36,57	9,79	27,68	8,61
Groningen	32	19	13	32,97	11,19	25,78	9,27
Utrecht	23	13	10	35,46	9,78	25,28	6,08
Goetingen	36	29	7	32,06	9,81	25,61	8,16
Tuebingen	9	4	5	32,11	9,37	23	0
Lille	18	11	7	33,89	7,65	22,89	2,59
Cobre	72	58	14	38,17	13,89	23,61	5,95
TOTAL	218	154	64	35,3	11,42	24,83	5,06

6. SUPPLEMENTARY BIBLIOGRAPHY

1. Bell MD, Lysaker PH, Beam-Goulet JL, Milstein RM, Lindenmayer J-P. Five-component model of schizophrenia: assessing the factorial invariance of the positive and negative syndrome scale. *Psychiatry research*. 1994;52(3):295-303.
2. Lindenmayer J-P, Grochowski S, Hyman RB. Five factor model of schizophrenia: replication across samples. *Schizophrenia Research*. 1995;14(3):229-34.
3. White L, Harvey PD, Opler L, Lindenmayer J. Empirical assessment of the factorial structure of clinical symptoms in schizophrenia. *Psychopathology*. 1997;30(5):263-74.
4. Bzdok D, Yeo BT. Inference in the age of big data: Future perspectives on neuroscience. *NeuroImage*. 2017;155:549-64.
5. Charrad M, Ghazzali N, Boiteau V, Niknafs A, Charrad MM. Package 'NbClust'. *Journal of Statistical Software*. 2014;61:1-36.
6. Hastie T, Tibshirani R, Friedman J. *The elements of statistical learning*. 2001. 2001.
7. Tibshirani R, Wainwright M, Hastie T. *Statistical learning with sparsity: the lasso and generalizations*: Chapman and Hall/CRC; 2015.
8. Pedregosa F, Varoquaux G, Gramfort A, Michel V, Thirion B, Grisel O, et al. Scikit-learn: Machine learning in Python. *Journal of Machine Learning Research*. 2011;12(Oct):2825-30.
9. Blanchard JJ, Cohen AS. The structure of negative symptoms within schizophrenia: implications for assessment. *Schizophrenia Bulletin*. 2006;32(2):238-45.

Acknowledgment

First and foremost, I am deeply grateful to my supervisor Danilo Bzdok for pushing me to bring out the best in me. His high expectations, thoughtful insights, strong passion and steady commitment were very effective to make my PhD journey very fruitful and unique. His culture of continuous learning and strong work ethic are aspects of Danilo's supervision that I admire and plan to emulate.

Special thanks to the IRTG 2150. I had the opportunity to learn, teach, present my work, get involved into different labs, strengthen and expand my network and drink wine on a rooftop terrace in Philly thanks to this research group. I would also like to convey thanks to the DFG for providing the financial means.

I would like to thank our co-authors for their great insights and supportive comments. I am eager to collaborate even more on new projects.

Many thanks to A. Elbakyan for what she's doing for science. Sincere thanks to all free and open-source software developers (with a big "hats off" to the Python community). I also thank everyone involved in the open-science flow: this is such an inspiring vision.

I would like to thank Germany, the city of Aachen and the RWTH university for welcoming me. It was great to connect with the German language and culture.

Deepest gratitude to my colleagues & friends in the shared office, in the UKA and elsewhere with a special big up to Marcel who followed me from begining to end. Thanks for their encouragement, assistance and time.

I wish to express my love and gratitude to my family, especially to my life-coach and mom Bernadette.

Finally, it is hard to find words to express how lucky I am to have met Juliette. I love my life so much with you.

Cheers and thanks again, to all of you.

Erklärung § 5 Abs. 1 zur Datenaufbewahrung

Hiermit erkläre ich, dass die dieser Dissertation zu Grunde liegenden Originaldaten

- bei mir, Lefort-Besnard Jeremy, 21 Rochusstraße, 52062 Aachen, Germany
und
- bei meinem Betreuer, Prof. Dr. Dr. Danilo Bzdok, Klinik für Psychiatrie, Psychotherapie und Psychosomatik, des Universitätsklinikums Aachen,

hinterlegt sind.

Affidavit according to § 5 (1) and (2), and § 11 (3) 12 of the doctoral studies

regulations

I, Lefort-Besnard Jeremy, hereby declare on oath, that I have contributed a significant part, and thus majority, of the publication:

Lefort-Besnard J. (candidate), Bassett S.D., Smallwood J., Margulies S.D., Derntl B., Gruber O., Aleman A., Jardri R., Varoquaux G., Thirion B., Eickhoff B.S., Bzdok D. (supervisor): Different shades of default mode disturbance in schizophrenia: Subnodal covariance estimation in structure and function; Human Brain Mapping; 2017, 39:644–661.

The contributions to the publications were as follows:

Names ->	Candidate: Jeremy Lefort- Besnard	Danielle Bassett	Jonathan Smallwood	Daniel Margulies	Birgit Derntl	Oliver Gruber	Andre Aleman	Renaud Jardri	Gael Varoquaux	Bertrand Thirion	Simon Eickhoff	Co-Authors	Doctoral supervisor: Danilo Bzdok	Sum (%)	
Study supervision														100	100
Study design/conception														100	100
Data manipulation	50													50	100
Data visualization	50													50	100
Vizualization insights		10	10	10	10	10	10	10	10	10	10	100			100
Statistical evaluation	50													50	100
Statistical insights		10	10	10	10	10	10	10	10	10	10	100			100
Delivery of materials					12,5	12,5	12,5	12,5					50	50	100
Interpretation of data evaluation	80	1	1	1	1	1	1	1	1	1	1	10	10	10	100
Writing/draft of the manuscript	100														100
Correction of the manuscript			1	1	1	1	1	1	1	1	1	10		90	100

The position as the first author obviously arises from this significant contribution.

Signature of the doctoral candidate

As supervisor and corresponding author I confirm the statements of Lefort-Besnard Jeremy and as a representative of the collaborative partners (Bassett S.D., Smallwood J., Margulies S.D., Aleman A., Jardri R., Varoquaux G., Thirion B.)

Signature of the doctoral supervisor

As co-author I endorse the statement of Prof. Dr. Dr. Bzdok
Names and signatures of all German speaking co-authors (allowed on separate pages)

Birgit Derntl

Oliver Gruber

Simon Eickhoff

Affidavit according to § 5 (1) and (2), and § 11 (3) 12 of the doctoral studies regulations

I, Lefort-Besnard Jeremy, hereby declare on oath, that I have contributed a significant part, and thus majority, of the publication:

Lefort-Besnard J. (candidate), Varoquaux G., Derntl B., Gruber O., Aleman A., Jardri R., Sommer I., Thirion B., Bzdok D. (supervisor): Patterns of Schizophrenia Symptoms: Hidden Structure in the PANSS Questionnaire; Translational Psychiatry; In press.

The contributions to the publications were as follows:

Names ->	Candidate: Jeremy Lefort-Besnard	Gael Varoquaux	Birgit Derntl	Oliver Gruber	Andre Aleman	Renaud Jardri	Iris Sommer	Bertrand Thirion	Co-Authors	Doctoral supervisor: Danilo Bzdok	Sum (%)
Study supervision											100
Study design/conception											100
Data manipulation	50										50
Data visualization	50										50
Vizualization insights		14,3	14,3	14,3	14,3	14,3	14,3	14,3	100		100
Statistical evaluation	50										50
Statistical insights		14,3	14,3	14,3	14,3	14,3	14,3	14,3	100		100
Delivery of materials			10	10	10	10	10	10		50	50
Interpretation of data evaluation	80	1,43	1,43	1,43	1,43	1,43	1,43	1,43	10	10	100
Writing/draft of the manuscript	100										100
Correction of the manuscript		1,43	1,43	1,43	1,43	1,43	1,43	1,43	10	90	100

The position as the first author obviously arises from this significant contribution.

Signature of the doctoral candidate

As supervisor and corresponding author I confirm the statements of Lefort-Besnard Jeremy and as a representative of the collaborative partners (Varoquaux G., Aleman A., Jardri R., Sommer I., Thirion B.)

Signature of the doctoral supervisor

As co-author I endorse the statement of Prof. Dr. Dr. Bzdok
Names and signatures of all German speaking co-authors (allowed on separate pages)

Birgit Derntl

Oliver Gruber